Science of the Total Environment 1001 (2025) 180470

Contents lists available at ScienceDirect

Science of the Total Environment

journal homepage: www.elsevier.com/locate/scitotenv

Phytoremediation by rooted macrophyte *Vallisneria spiralis*, not biochar amendment, reduces eutrophication from nutrient release in organic-rich sediment of a polluted wetland

Leonardo Morini [a,b], Claudio Ferrari [b,*], Monia Magri [b], Sara Benelli [b], Mindaugas Zilius [c], Giovanna Visioli [b], Marco Bartoli [b]

[a] Department of Environmental and Prevention Sciences, University of Ferrara, Via Luigi Borsari 46, Ferrara, 44121, Italy
[b] Department of Chemistry, Life Science and Environmental Sustainability, University of Parma, Parma, Italy
[c] Marine Research Institute, Klaipeda University, 92295, Klaipeda, Lithuania

HIGHLIGHTS

- *Vallisneria spiralis* influences nitrification and denitrification in the sediment.
- Biochar and *V. spiralis* do not negatively interact.
- Phytoremediation is more efficient to decrease nutrient release compared to biochar.
- *V. spiralis* shapes the benthic microbial community composition and functioning.

GRAPHICAL ABSTRACT

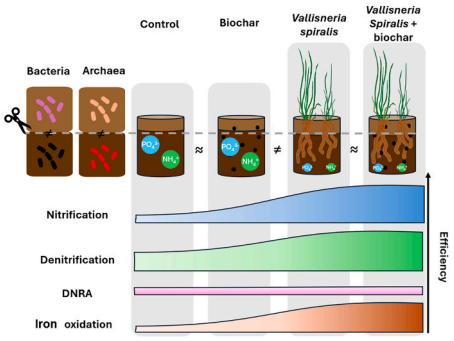

ARTICLE INFO

Keywords:
Benthic microbial community
Nitrogen cycle
Metabolic rates
Radial oxygen loss
Phytoremediation
Biochar
Vallisneria spiralis

ABSTRACT

Wetlands sediments are often contaminated by macro and micropollutants. Combined traditional and biochar assisted phytoremediation techniques allow contrasting of both pollutants. However, the interacting effects of different techniques are seldom analysed, assuming that they are null or positive. We investigated phytoremediation by the macrophyte *Vallisneria spiralis* and biochar addition in polluted sediments. The aim was to assess if biochar affects the biogeochemical services provided by the macrophyte via radial oxygen loss and nutrient uptake. Sedimentary fluxes and properties, and microbial activity and diversity were analysed in four conditions: control sediments, sediments with *V. spiralis*, sediments with biochar and with both *V. spiralis* and biochar. Sediments with *V. spiralis* had higher redox and Fe^{3+} solid pools and had lower pore water concentrations of NH_4^+ and PO_4^{3-} than control sediments. Sediment with macrophytes had lower denitrification, higher nitrification and similar nitrate ammonification potential than bare sediment. The screening of microbial diversity suggests distinct communities in surface and subsurface sediments, regardless of the presence of macrophytes or biochar. The presence of *V. spiralis* roots stimulated slow growing groups of microbes as nitrifiers, iron and sulphide oxidizers or promoted the switch to aerobic metabolism without affecting microbial diversity

* Corresponding author.
E-mail address: claudio.ferrari1@unipr.it (C. Ferrari).

https://doi.org/10.1016/j.scitotenv.2025.180470
Received 17 June 2025; Received in revised form 8 September 2025; Accepted 8 September 2025
Available online 22 September 2025

and abundance. Biochar addition, likely due to low reactivity and 30 days incubation time, did not affect pore water nutrients, microbial activity and diversity, suggesting limited remediation in the organic-polluted sediments considered. Biochar also did not affect the biogeochemical ecosystem services provided by *V. spiralis*, suggesting the absence of negative interactions between the two treatments.

1. Introduction

Freshwater wetlands in densely inhabited areas are threatened by multiple stressors, resulting in loss of biodiversity and functioning and accumulation of macro and micropollutants (Vörösmarty et al., 2010). Restoration actions may simultaneously employ different techniques to be effective and improve the ecological status of wetlands. The transplant of macrophytes, or any action that favours their colonization, generally targets the removal of nutrients and the oxygenation of both water and sediment, whereas the addition of adsorbing materials to the sediments targets the immobilization of microcontaminants as heavy metals or hydrocarbons (Galitskaya et al., 2016). Biologically-mediated remediation techniques, which are generally effective in the long-term, can be applied at sites already subjected either to passive remediations or containment actions that are fast to deploy and easy to manage (Zamparas and Zacharias, 2014). An example of a combined remediation approach in polluted wetlands is the immobilization of contaminants by active materials, followed by phytoremediation to decrease nutrient loading and eutrophication risk (Deng et al., 2021). While different studies analysed in detail the effectiveness of either macrophytes or active materials on the removal or retention of a variety of chemicals, a few studies evaluated if the simultaneous application of different remediation techniques generates interactive effects (Liu et al., 2023). Such interactive effects would either amplify or reduce the expected additive effects of the different remediation actions.

Aquatic plants provide multiple biogeochemical ecosystem services; hence they are frequently used as nature-based solutions to restore impacted areas and improve their chemical and biological quality (Thomaz, 2023). In the water column they create habitat and niches, favouring macrofauna and fish diversity, they expand with their stems and leaves the interfaces for biofilm growth, they produce O_2 and promote transparency (Thomaz, 2023). Aquatic plants fix carbon and assimilate nutrients from the water column and from the pore water. As such, they can control phytoplankton growth and limit internal recycling from sediments (Soana et al., 2015). Macrophytes also have a large potential to change different critical aspects of the sedimentary environment, such as O_2 limitation and chemically reduced conditions. Indeed, one of the adaptive strategies of aquatic plants that enables roots survival in anoxic sediments is radial oxygen loss (ROL) (Colmer, 2003). ROL consists in the leakage of O_2 from roots to the nearby rhizosphere, where it establishes oxic and suboxic microenvironments that allow plant growth and survival (Sand-Jensen et al., 1982). The oxidized sediment volume generated by ROL represents a buffer that protects roots from the phytotoxic effects of sulphides and heavy metals, which are frequently abundant in anoxic conditions and in contaminated sediments (Colmer, 2003). Besides ensuring plant survival and growth, ROL generates numerous indirect effects on the benthic compartment: it affects microbial diversity and favours aerobic microbial processes in the rhizosphere (Vila-Costa et al., 2016;), it enhances nitrification and subsequently denitrification along oxic-anoxic microgradients within the rhizosphere (Morini et al., 2024; Racchetti et al., 2017; Risgaard-Petersen and Jensen, 1997) and it favours the precipitation of iron oxyhydroxide plaques and the coprecipitation of phosphorus on the roots surface (Magri et al., 2023). ROL can significantly decrease the emission of methane from organic-polluted sediment, either due to inhibition of methanogenesis or to the increase of methane oxidation. ROL can finally promote the mineralization of refractory organic matter via aerobic microbial heterotrophic metabolism or facilitate the activity of deposit-feeding macrofauna. All these effects directly or indirectly improve the sediment buffer capacity against the build-up of potentially toxic compounds in the pore water and their release to the water column and enhance the nutrient sink role of sediment, the coupling of organic matter input and mineralization processes, and the reduction of greenhouse gas emissions to the atmosphere.

Among adsorbing materials, biochar represents a widely employed material for soil and sediment remediation. Biochar is a low-cost carbonaceous material produced by partial combustion of biomasses under anaerobic conditions. Biochar increased the interests of researchers and stakeholders in the last decade for its effectiveness as a soil amending agent and for its capacity to immobilize organic pollutants and heavy metals (Amalina et al., 2024). Biochar enhances the degradation and mineralization rates of organic pollutants thanks to the catalytic effects of its active surface groups. Differently, the ability of biochar to trap nutrients in its matrix and enhance microbially-mediated mineralization processes is still debated and dependent upon both biochar and sediment characteristics (Wei et al., 2023; Zhao et al., 2022). Biochar, due to its negative charges and high cation exchange capacity, traps more efficiently NH_4^+ rather than NO_3^-. Sometimes, biochar also enhances the precipitation of phosphate (PO_4^{3-}) due to the presence on its surface of coordinated cations as Ca^{2+} and Mg^{2+} (Cui et al., 2016). Furthermore, biochar may indirectly enhance microbially-mediated processes by favouring bacterial growth, with effects on nutrient cycling and hydrocarbon decomposition efficiency (Galitskaya et al., 2016). The capacity of biochar to buffer sediment toxicity may indirectly enhance the health, growth rates, and remediation efficiency of rooted macrophytes and the rhizosphere-associated microbial community (Liu et al., 2023). The latter may simultaneously lead to higher mineralization, nutrient accumulation in pore water, and recycling in the water column, smoothing the macrophyte sink role for nutrients and benthic nutrient trap. Biochar may also change the sediment physical properties, potentially limiting macrophyte growth, whose optimal environmental conditions are generally narrow (Risgaard-Petersen and Jensen, 1997).

Combined experiments to evaluate the interaction of macrophytes and biochar in the remediation of sediments mainly focused on heavy metals and organic pollutants (Boucher-Carrier et al., 2022). Studies evaluating the interacting effects of the two treatments on nutrient reduction are comparatively scanty (Zheng et al., 2021). This study aimed to test whether the biogeochemical services provided by submersed macrophytes in organic sediments are affected by the presence of biochar and if this interaction is positive or negative. Research questions focus on ecosystem services promoting nutrient removal or retention, which include assimilation, the creation of oxidized niches within the anoxic sediment matrix, and the stimulation of both aerobic (e.g., via ROL) and anaerobic microbial communities (e.g., via exudates). We hypothesized positive interacting effects of biochar and macrophytes, as biochar is expected to provide multiple interfaces for microbial growth, resulting in higher organic matter mineralization and nutrient recycling in a more oxidized matrix. We also hypothesized different microbial growth and community composition across treatments due to the interplay of macrophytes and biochar. To this purpose, pore water pH and Eh and nutrient concentrations, sedimentary fluxes, iron pools, and microbial activity and diversity were analysed in reconstructed microcosms containing organic sediments, sediments added with the submersed macrophyte *Vallisneria spiralis*, sediments added with biochar, and sediments added with both *V. spiralis* and biochar.

2. Methods

2.1. Sediment and macrophyte sampling and biochar features

The sediments used in the experiment were collected from the central portion of the Vallazza site, a riverine wetland bordering the Mincio River (Mantua, northern Italy). The chosen area is a hotspot of pollution within a Site of National Interest (SIN), an area that Italian law classifies as highly contaminated and either undergoing, or requiring, remediation. The Vallazza sediments are contaminated by aromatic organic compounds and heavy metals released since 1960s by the nearby industrial hub, hosting a petrochemical plant and a refinery. They also receive organic matter inputs coming from the effluents of the Mantua city wastewater treatment plant, serving 100,000 inhabitant equivalents.

In December 2022, nearly 300 L of in situ water and 40 L of surficial sediments (0–20 cm horizon) were collected from the shallow (1 m water depth) central portion of the Vallazza SIN (45°08′01.6″ N 10°48′34.6″ E). Sediments represented an integrated sample of 40 pooled intact surficial sediment were randomly collected (i.e. 5 cm) within an area of 300 m^2 using poly(methyl methacrylate) (PMMA) liners mounted on a hand corer. Sediments were immediately extruded and pooled in a tank. The sediments were black along the upper vertical profile, without colour gradients or clear evidence of bioturbation. They were brought to the laboratory and sieved (1 mm mesh) to remove large debris and macrofauna, consisting of a few chironomid larvae. The sieved sediment settled in the dark inside an open tank. After 24, 48 and 72 h, the overlying water was syphoned off until the water accumulation over the sediment was negligible. At this point the sediment was transferred into experimental microcosms, as described below.

In addition to polluted sediments, ~100 individuals of the submersed rooted macrophyte *Vallisneria spiralis* (Hydrocharitaceae) were collected from a littoral site of the Mincio River, upstream of the SIN (45°16′42.3″ N, 10°42′29.9″ E). Vegetated sediments were also muddy and organic, but their colour was light brown. Collected plants were rinsed with in-situ water to remove sediments from roots and epiphytes and macrofauna from leaves. Previous studies evidenced how *V. spiralis*, colonizing organic littoral sediments upstream Vallazza site, can also grow in organic-polluted sediment (Morini et al., 2024).

Biochar was obtained from hardwood and wood pellets through pyrogasification at a temperature between 400 and 500 °C and subsequently ground and sieved. The final product had an organic matter content of 91.0 ± 0.1 %, and a content of total carbon, nitrogen and phosphorus of 77 ± 7 %, 0.0034 ± 0.0008 %, and 0.194 ± 0.003 %, respectively. The low N content and extremely high C/N molar ratio (~19,000) are characteristic features of biochar produced at high temperature. The heavy metals and PAHs content was lower than the national regulation limit for all the parameters investigated. The complete analytical report of the biochar characterization is provided as supplementary material (S2).

2.2. Experimental setup

The sieved sediments were transferred into 28 bottom-capped cylindrical PMMA microcosms (inner height = 9 cm, inner diameter = 7 cm, volume = 346 cm^3). Half of the microcosms were amended with 10 g of dry biochar, homogeneously mixed in the sediment to a final concentration of 27.3 mg cm^{-3}. The microcosms were wrapped with aluminium foil to avoid light contamination and photosynthesis along the microcosm wall. Two individuals of *V. spiralis* were transplanted in 14 microcosms (7 amended with biochar and 7 without biochar addition), simulating an in-situ plant density of 520 individuals m^{-2}. All plants had similar size, number of leaves, and root volume. Individuals of *V. spiralis* are easily manipulated and are not affected by transplant, even in organic-enriched sediments (Soana et al., 2015). A total of four treatments were created, with 7 replicates each: control bare sediment (C), sediment with biochar (CB), vegetated sediment (P) and vegetated sediment with biochar (PB). Once created, all microcosms were submerged and pre-incubated in a temperature-controlled aquarium (15 ± 2 °C) containing 100 L of unfiltered, aerated, and stirred in situ water. All microcosms underwent a 30 days preincubation period under a 12 h of light and 12 h of dark daily cycle to allow: (1) the establishment of stable chemical gradients between the water and sediment phases (Zhang et al., 2010; Magri et al., 2023; Morini et al., 2024), and (2) the growth of microbial communities (Stocum and Plante, 2006). The irradiance of the halogen lamp used for the light phase was set at ~400 μE m^{-2} s^{-1}. About 20 % of the tank water was renewed with fresh in-situ water every 4 days to maintain nutrient concentrations and chemical gradients across the sediment-water interface as close as possible to in situ conditions.

After the preincubation period, we randomly chose microcosms from the aquarium (4 per treatment, $n = 16$ microcosms, SET_1) and incubated them at controlled conditions to measure net fluxes of dissolved O_2 and inorganic nutrients at the sediment-water interface. After the incubation procedure, sediments from SET_1 were characterised for pH and redox potential, pore water chemistry, and chlorophyll *a*, whereas plants from SET_1 were analysed for their dry weight and C and N elemental content (both roots and leaves) and size (only leaves). The remaining microcosms (3 per treatment, $n = 12$, SET_2) were used to collect surface and subsurface sediments (0–1 and 1–5 cm depth, respectively) to quantify potential microbial activity, (nitrification, denitrification and nitrate ammonification), sediment features (density, organic content, C and N elemental composition, iron mineral content), and the bacterial and archaeal communities' composition. A schematic representation of the experimental design is provided in the Supplementary Fig. S2.

2.3. Benthic fluxes measurement

After the preincubation period, SET_1 microcosms were carefully included in PMMA liners underwater (Racchetti et al., 2017). As microcosms in the aquarium were placed on rubber stoppers, the latter were also included in the liners, which became bottom capped. The top of the liners remained open to allow the exchange of aerated and mixed water from the Vallazza site. Each liner was provided with a Teflon-coated magnet suspended in the water column and driven by an external unit rotating at 40 rpm. This speed enables the mixing of the water, avoiding resuspension of the sediment inside the microcosms. The liners containing *V. spiralis* were also provided with a plastic net (1 cm mesh size) between the leaves and the magnet. This net avoids damage to the plants and interference with the magnet's rotation during the incubation by the leaves, while still ensuring the same water mixing (Fig. S1). The microcosms were then incubated under dark and light conditions by capping the liners with opaque or transparent lids, as detailed in Magri et al. (2023). Dark and light short incubations (4 h) were carried out on December 19 and 20, 2022, respectively. The water temperatures during the incubations were 14.0 ± 1.0 °C and 17.0 ± 0.5 °C. In between incubations, the liners were maintained with the top uncapped and submersed in renewed in situ water to restore chemical gradients. Light incubations were carried out using the same halogen lamps used during preincubation and set at the same irradiance of 400 μE m^{-2} s^{-1}. Following pilot tests, the incubation time was set to maintain dissolved oxygen concentration in the water column within ±30 % of the initial value. Dissolved O_2 concentration was measured at the beginning and at the end of the incubation, with a Clark-type microsensor (Ox-50, Unisense A/S) connected to an amplifier (Microsensor Multimeter, Unisense A/S). Water samples for dissolved nutrient analyses (nearly 30 mL) were collected from each liner just before the start and at the end of the incubation with plastic syringes. An aliquot of 20 mL was filtered (Whatman GF/F, glass fiber filters) and stored at −20 °C in plastic vials for the spectrophotometric analyses of NH_4^+ and dissolved reactive silica (DRSi) (APHA et al., 2005). Another aliquot of 10 mL was filtered (Whatman GF/F) and immediately analysed for the

spectrophotometric determination of soluble reactive phosphorus (PO_4^{3-}) (Valderrama, 1981). Dissolved O_2 and inorganic nutrient fluxes were calculated according to the equation below:

$$F_x = \frac{(C_f - C_i)V}{A\Delta t}$$

where F_x is the flux of the solute x (μmol m^{-2} h^{-1}), C_f and C_i are the final and initial concentrations of the solute x (μM), V is the volume of the water overlying the sediment contained in the liner, A is the sediment surface area (m^2) and Δt is the incubation time (h). Positive and negative fluxes indicate an increase and a decrease of the concentration of a solute in the water phase, respectively. Dissolved O_2 fluxes in the dark and in the light account for microcosms' net respiration (R) and primary production (NPP), respectively. Gross primary production (GPP) was calculated as: GPP = NPP − R, considering photorespiration as negligible. Daily fluxes were calculated by multiplying dark and light hourly fluxes by 12 and summing the obtained values.

2.4. Sediments and macrophytes characterization

Following the incubations, SET_1 microcosms were removed from the liners underwater leaving them submersed in the incubation tank for 24 h. The day after, we inserted in each microcosm a combined pH electrode (Radiometer), a platinum Eh electrode (Hamilton) and a Rhizon® (Rhyzosphere Research Products, CSS 19.21.23F). The pH and Eh electrodes reached 2.5 cm below the sediment-water interface to allow comparison of sediment pH and redox potential across treatments in a subsurface sediment layer with high root density. The Rhizon explored the whole 0–5 cm depth sediment layer to allow comparison of pore water chemistry (inorganic nutrients and dissolved Fe and Mn) across treatments. An aliquot of the extracted pore water was immediately acidified with 50 μL of 70 % HNO_3 and stored in a 6-mL glass vial (Exetainer, Labco, High Wycombe, UK) for the analyses of dissolved Fe^{2+} and Mn^{2+} (atomic absorption, Varian, AA280 FS). An aliquot was stored at −20 °C in plastic vials for the analysis of NH_4^+ and DRSi and another one was immediately analysed for PO_4^{3-}, as previously detailed.

After the extraction of the pore water, 1 mL of fresh sediment was collected with a cut-off syringe from the upper 0–1 cm depth layer for chlorophyll *a* (chl a) determination. The pigment was extracted from the sediment with 5 mL of 90 % acetone, in the dark for 24 h at +4 °C and determined spectrophotometrically after centrifugation (Lorenzen, 1967).

The leaves of *V. spiralis* were cut off, gently washed to remove epiphytes, and weighed wet and dry (60 °C until constant weight). The dry leaves were ground with a ceramic mortar and pestle for subsequent quantification of total organic carbon (TOC) and total nitrogen (TN) with an elemental analyser (FlashEA 1112, Thermo Electron Corporation) at the Center for Physical Sciences and Technology (Lithuania), after removing carbonates with 1 M HCl.

The roots were gently removed from the microcosms and rinsed them with water to remove residual sediment particles. The roots were inserted in 40 mL gas-tight glass vials filled with 20 mL of 0.5 M HCl and maintained on a shaker for 16 h at 25 °C. This procedure allows the quantification of the Fe and Mn coating the roots surface (Magri et al., 2023). After the extraction, the roots were removed from the vials, and the remaining acidic extract was diluted for the analysis of dissolved Fe and Mn via atomic absorption. The roots were then neutralized with distilled water and analysed for TOC and TON as previously described for the leaves.

2.5. Measurements of N-related microbial activities

The sediment from SET_2 microcosms was analysed by separating it into two different layers (0–1 cm and 1–5 cm depth) to distinguish the upper horizon, where O_2 can diffuse, from the subsurface horizon which is typically anoxic if not for the presence of roots or burrowing macrofauna. A sediment aliquot from each layer was used to quantify potential rates of microbial nitrification (PN), denitrification (PD) and dissimilative nitrate reduction to ammonium (PDNRA) and to characterize microbial diversity. To this purpose, a cut-off syringe was vertically inserted in each microcosm to retrieve a 5-cm thick sediment column. From such syringes, two sediment slices (1–5 cm and 0–1 cm depth) were extruded, then homogenized with a sterilized spatula and subsampled (2 mL) for oxic (nitrification) and anoxic (nitrate reductions) slurry incubations.

Twenty-four oxic slurries were prepared to investigate potential nitrification rates (3 replicates for each treatment x 4 treatments × 2 sediment layers). To this purpose, 2 mL of sediment were suspended in an Erlenmeyer flask containing 40 mL of 0.22-μm filtered in-situ water added with NH_4^+ concentrated solution to a final concentration of 200 μM. The flasks were maintained for 20 h open in the dark, on a shaker at 25 °C. 5 mL of slurry were collected from every flask just before the start and at the end of the incubation. The collected samples were centrifuged at 4200 rpm for 3 min and the supernatant was filtered (Whatman GF/F) for subsequent analysis of NO_2^- and NO_3^- (APHA et al., 2005). The potential nitrification rate was calculated as:

$$PN = \frac{\left([NO_3^-]_f + [NO_2^-]_f\right) - \left([NO_3^-]_i + [NO_2^-]_i\right)}{\Delta t \rho}$$

where PN is the potential nitrification rates (nmol N-NO_3^- g^{-1} h^{-1}), Δt is the duration of the incubation (h) and ρ is the density of the slurry (g L^{-1}).

The potential rates of nitrate dissimilatory reductions were calculated using time series incubations ($n = 4$ incubation times) on 2 sets of anoxic slurries. In total, 192 slurries were prepared (3 replicates per treatment x 4 treatments × 2 layers × 4 sampling times × 2 target processes). All 192 slurries consisted of 12-mL glass vials (Exetainer, Labco, High Wycombe, UK) filled without headspace with 2 mL of sediments, 10 mL of filtered anoxic (N_2 saturated) in-situ water, and a glass bead. The procedure was carried out into a N_2-filled glove bag. The exetainers were placed on a rotating shaker in the dark and preincubated for 12 h to allow microbial respiration to consume any residual O_2 and $^{14}NO_3^-$. Thereafter, a solution of $^{15}NO_3^-$ (Merck, Sodium nitrate-^{15}N, >98 atom% ^{15}N) was injected in all 192 slurries with a 1-mL syringe through the rubber septum to a final concentration of ~200 μM. A second needle was inserted in the septum to allow overflow while injecting the $^{15}NO_3^-$. A subset of the slurries targeting denitrification potential ($n = 24$ out of 86) was immediately poisoned with 200 μL of 7 M $ZnCl_2$ after the $^{15}NO_3^-$ addition. The remaining three subsets were sequentially removed from the shaker at 3 h intervals and poisoned using the same procedure. Potential denitrification rate (PD, nmol N-N_2 g^{-1} h^{-1}) was calculated as:

$$PD = \frac{\delta C}{\delta t}\frac{1}{\rho}$$

where $\delta C/\delta t$ is the slope of the linear regression between the concentrations of the ^{15}N-N_2 produced and the incubation time divided by the density of the slurry ρ.A second subset of the slurries, specifically targeting DNRA, (n = 24 out of 86) was transferred in plastic tubes containing 1 g of KCl immediately after the $^{15}NO_3^-$ addition, mixed and centrifuged at 2700 rpm for 3 min. The supernatant was filtered (Whatman GF/F) and frozen into plastic vials until analysis. An aliquot was analysed for NH_4^+ using standard spectrophotometric methods (APHA et al., 2005). Another aliquot was bubbled with air for 3 min to remove ^{15}N-N_2 traces, transferred to 6 mL glass vials without headspace, capped and added with 100 μL of alkaline hypobromite solution to oxidize ^{15}N-NH_4^+ to ^{15}N-N_2 (Warembourg, 1993). A second needle was inserted in the cap septum to allow overflow. The same procedure was applied to 3 more slurry subsets that were terminated every 3 h. All samples were stored at 25 °C in the dark until analysis of N_2

concentration and isotopic ratio with a membrane inlet mass spectrometer (MIMS, Bay -Instruments). The production of $^{15}NH_4^+$ by DNRA was calculated as the slope of the linear regression between the concentration of $^{15}N\text{-}N_2$ and the incubation time multiplied by the dilution factor of the slurry.

Simultaneously 2 mL of fresh sediment from the upper (0–1 cm) and subsurface (1–5 cm) layers from SET_2 were transferred in 40-mL glass vials filled with 10 mL of 0.5 M HCl to avoid Fe^{2+} oxidation. The samples were subsequently analysed in triplicate for Fe^{2+} and microbially reducible Fe^{2+} with the ferrozine method (Lovley and Phillips, 1987). We collected another aliquot of 5 mL of fresh sediment with a cut-off syringe for the measurement of density, porosity and water content. These properties were calculated after weighing a known amount of sediment before and after desiccation (60 °C) until constant weight. An aliquot of powdered, dried sediment was analysed for organic matter content (OM) as a percentage of weight loss after ignition at 450 °C for 3 h. An aliquot was analysed for total carbon (TC) and total nitrogen (TN) content with an elemental analyser (FlashEA 1112, Thermo Electron Corporation) at the Center for Physical Sciences and Technology (Lithuania), after removing carbonates with 1 M HCl. An aliquot was analysed for total and organic phosphorus according to Aspila et al. (1976).

2.6. DNA extraction, sequencing and bioinformatics analysis

A minimum of 2 mL of fresh sediment was obtained from both the surface (0–1 cm) and subsurface (1–5 cm) layers using a sterile spatula. In total, we collected 24 samples (3 replicates × 2 sediment layers × 4 treatments) that were stored at −80 °C until DNA extraction.

Microbial DNA from 450 to 500 mg of homogenized sediment was extracted using the NucleoSpin Soil kit (Macherey-Nagel, Düren, Germany), following the manufacturer's protocol, which involved the use of lysis buffer SL1 and Enhancer solution SX. DNA was eluted in 50 μL of elution buffer SE. The quality of the DNA extraction was assessed via electrophoresis on a 1 % agarose gel, and DNA concentration was quantified using the dsDNA HS Assay Kit (0.2–100 ng μL^{-1}) on a Qubit 2.0 Fluorometer (Life Technologies, Carlsbad, CA, USA). The extracted DNA was subsequently sent to Novogene Europe (Cambridge, UK) for PCR amplification, library preparation, and sequencing.

For bacterial community composition analysis, The hypervariable V3-V4 region of the 16S rRNA gene was amplified using the universal primers 341F (5′-CCTAYGGGRBGCASCAG-3′) and 806R (5′-GGACTACNNGGGTATCTAAT-3′) and for the Archaeal community composition the V4-V5 region with primers Arch519F (5′-CAGCCGCCGCGGTAA-3′) and Arch915R (5′-GTGCTCCCCCGCCAATTCCT-3′). Multiplexed libraries with unique index tags were prepared by Novogene Europe, and sequencing was performed using Illumina NovaSeq 6000 platform, generating 250-bp paired-end raw reads (Raw PE), which were then merged and processed to obtain Clean Tags. Chimeric sequences were identified and removed to generate Effective Tags, which were used for subsequent analysis.

Before bioinformatics processing, the raw amplicon data was denoised and corrected for sequencing errors using DADA2 (Callahan et al., 2016). Primer sequences were removed by the sequencing facility before analysis. The effectiveness of the filtering process of both raw and filtered data was evaluated with FastQC 0.11.9 (Andrews, 2010) and aggregated them using MultiQC 1.12 (Ewels et al., 2016). The error model was configured with parameters: nbases = 1e8 and MAX_CONSIST = 30, and the merging step was performed with a minimum overlap of 10 base pairs. Chimera removal was carried out using the "consensus" method. Amplicon sequence variants (ASVs) were annotated using the SILVA nr99 v138.1 reference database (Quast et al., 2012), and sequences identified as singletons, chloroplasts, or mitochondria were excluded from the final ASV table. The resulting ASV data were normalized to relative abundances and analysed using Explicet 2.10.5 (Robertson et al., 2013). Shannon's H alpha diversity index for both bacterial and archaeal communities was calculated after subsampling to the smallest sample size (bacteria: 67,215 counts; archaea: 1120 counts) using Explicet 2.10.15.

2.7. Data analysis and statistics

All the statistical analyses and graphical representations were conducted with RStudio Version 2023.06.1 (RStudio, 2023). Normality of each variable was evaluated using the Shapiro-Wilk test (function: *shapiro.test*). Equality of variance between different groups was assessed performing Levene's test (function: leveneTest from package *car*). When data were normally distributed with homogeneous variances, a two-sample *t* or analysis of variance (ANOVA) tests was employed to determine if treatments or sediment layers differed significantly ($p \leq 0.05$). Tukey's HSD test (function: TukeyHSD) was performed after ANOVA to conduct pairwise comparisons. If normality assumptions were not met, we used non-parametric Mann-Whitney U (two samples) or permutational analysis of variance PERMANOVA (three or more samples) tests. PERMANOVA was performed with adonis2 function (Rstudio, package *vegan*) based on the Bray-Curtis dissimilarity index. The *p*-value was determined after 999 permutations and set at $p \leq 0.05$. Pairwise PERMANOVA (pairwise adonis function in R, package *pairwiseAdonis*) based on the Bray-Curti's dissimilarity index was subsequently performed to investigate significance between single treatments. Correlations among sediment features and measured processes were analysed with Pearson's *r* correlation index. The correlation index was calculated for PN and bacterial genera performing nitrification, PD and bacterial genera performing denitrification, Fe^{3+} to total Fe pool ratio and iron reducing and oxidizing genera. The ecological distance between bacterial and archaeal communities in different replicates and treatments was assessed by performing a two-dimensional non-metric multidimensional scaling (NMDS function in R, package *vegan*) using distance matrix based on Bray-Curtis' dissimilarities of the bacterial abundances.

3. Results

3.1. Sediment physical and chemical properties and V. spiralis characterization

Sediment density and porosity were not significantly affected by the presence of *V. spiralis* and/or biochar (ANOVA, $p > 0.10$) and averaged 1.05 ± 0.06 g cm^3 and 0.88 ± 0.04, respectively. The OM content of control sediment and of sediment added with biochar were 23.1 ± 0.5 wt% and 29.2 ± 4.0 wt%, respectively (Table 1). The addition of biochar increased the total sedimentary C and slightly decreased TP and TN (Table 1), leading to a significantly higher C to N ratio, by a factor of 2, in biochar-amended (21.1 ± 2.45) versus control sediments (9.2 ± 0.8). The solid phase Fe^{3+} to Fe^{2+} ratio was higher in vegetated as compared to control sediment, especially in the 0–1 cm layer (Fig. 1). Biochar did not produce any significant effects on the total Fe pool and its oxidation status.

After the pre-incubation period, transplanted individuals of *V. spiralis* had new leaves and propagules and did not show any sign of stress. TC and TN in the leaves were 33.24 ± 0.99 and 3.03 ± 0.09 wt% of the dry mass, respectively, whereas TC and TN in roots averaged 41.75 ± 3.59 and 3.05 ± 0.30 wt%, respectively. Only the TC was significantly different between leaves and roots ($p < 0.05$), leading to a C:N ratio of the roots (16.0) 25 % higher than in leaves (12.8). The roots surface was covered by solid plaques with an iron and manganese content of 838 ± 477 and 28 ± 13 μmol g^{-1} of dry root mass, respectively. The chl-a concentration in the superficial sediment layer was significantly higher in the presence of *V. spiralis* (9.2 ± 0.4 mg m^2) as compared to control sediments (8.2 ± 0.1 mg m^2, $p < 0.01$), likely due to epiphytes detached from the leaves.

In unvegetated sediments, pore water PO_4^{3-} and NH_4^+ concentrations were ~10 fold and ~50 fold higher, respectively, than in microcosms

Table 1
Physical and chemical properties of the sediment investigated.

Treatment	Layer	Density	Porosity	Porosity	Organic matter	C total	N total	P total	P organic
	cm	g cm^{-3}		wt%	wt%	wt%	wt%	μmol g^{-1}	μmol g^{-1}
Control	0–1	1.08 ± 0.02	0.93 ± 0.02	86.62 ± 0.69	22.59 ± 0.45			661.6 ± 43.4	276.2 ± 68.3
	1–5	1.06 ± 0.0	0.89 ± 0.04	84.09 ± 0.49	23.12 ± 0.26	17.06 ± 2.09	1.95 ± 0.09	692.1 ± 81.0	193.8 ± 116.6
Biochar	0–1	1.00 ± 0.08	0.85 ± 0.07	84.7 ± 0.35	36.15 ± 6.04			685.6 ± 76.3	326.1 ± 56.2
	1–5	1.03 ± 0.04	0.85 ± 0.02	82.03 ± 1.47	31.05 ± 2.97	36.14 ± 7.38	1.53 ± 0.17	673.1 ± 93.	395.8 ± 31.7
V. spiralis	0–1	1.00 ± 0.03	0.88 ± 0.02	87.96 ± 0.3	23.17 ± 0.48			641.8 ± 108.6	197.6 ± 108.1
	1–5	1.04 ± 0.08	0.87 ± 0.07	83.17 ± 0.12	23.49 ± 0.35	36.14 ± 7.38	1.91 ± 0.05	674.3 ± 73.0	142.4 ± 91.4
Biochar + *V. spiralis*	0–1	1.04 ± 0.03	0.9 ± 0.03	86.02 ± 1.19	29.37 ± 1.75			632.2 ± 62.1	266.0 ± 6.3
	1–5	1.12 ± 0.01	0.91 ± 0.00	81.27 ± 0.47	33.86 ± 1.05	29.04 ± 3.48	1.62 ± 0.05	555.7 ± 79.1	258.63 ± 105.4

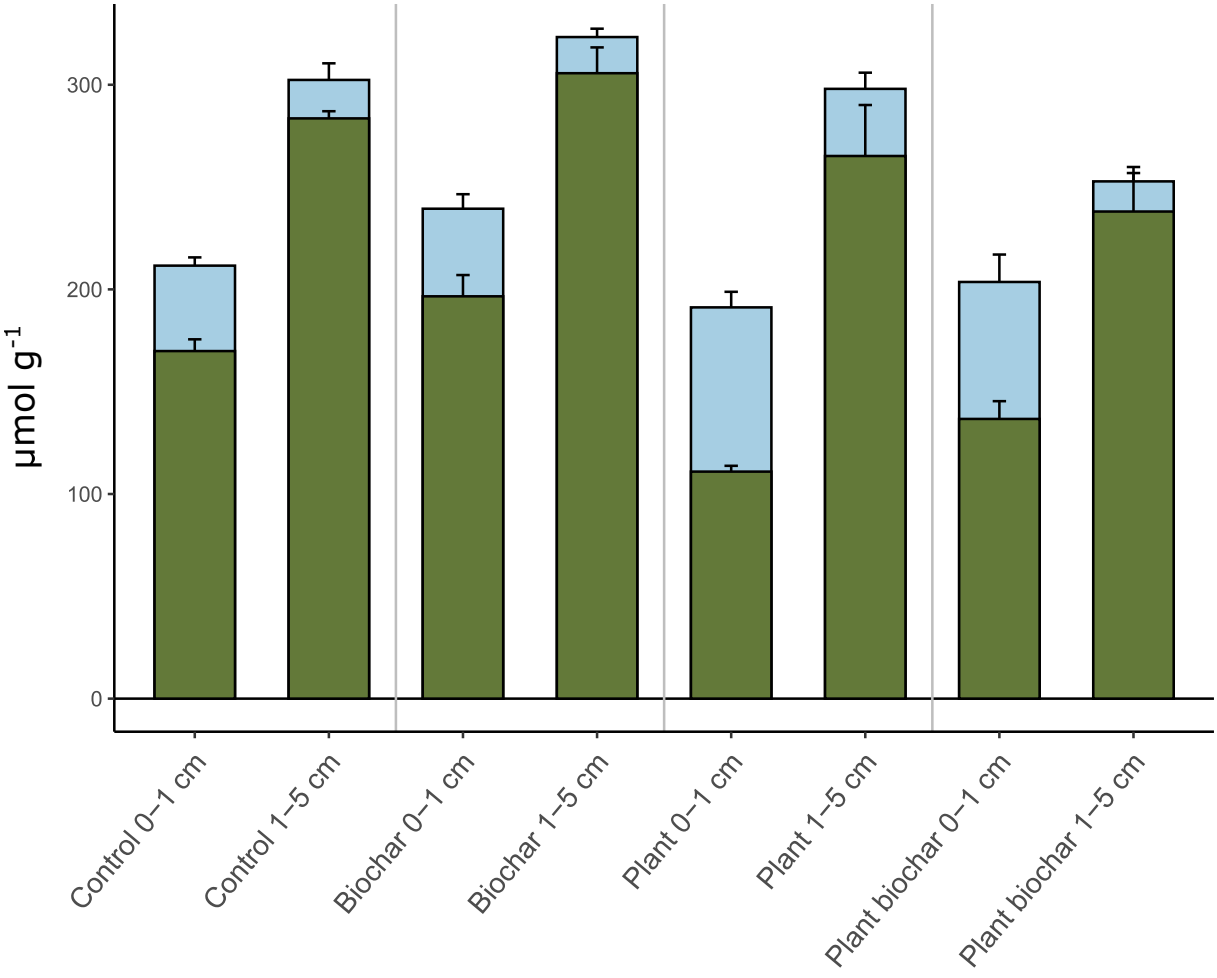

Fig. 1. Green bars represent the Fe^{2+} pool and the blue bars the microbially reducible Fe^{3+} pool. Together, they account for the total microbially reactive iron pool in the sediments.

with *V. spiralis*, respectively, regardless of biochar presence ($p < 0.001$; Fig. 2a, b). Biochar did not affect (i.e., neither increased nor decreased) pore water concentration of both nutrients compared to control sediment (Fig. 2a, b). Conversely, DRSi concentration was influenced by both *V. spiralis* and biochar ($p < 0.01$). The macrophyte induced a decrease of DRSi by 24 %, whereas the biochar produced an increase of 18 % compared to control microcosms (Fig. 2c). The pore water of vegetated sediments was depleted in dissolved Fe and Mn (Fig. 2d, e). Microcosms with both *V. spiralis* and biochar had significantly lower sediment pH (7.57 ± 0.07) than control sediments and sediments with *V. spiralis* or biochar (8.05 ± 0.08; $p < 0.05$; Fig. 2f). The Eh measured in vegetated sediments was always positive (+227 ± 79 mV), whereas it was negative in the absence of plants (−48 ± 16 mV). Eh was not affected by biochar addition ($p > 0.1$) but only by *V. spiralis* ($p < 0.05$) (Fig. 2g).

3.2. Diffusive fluxes and potential rates of denitrification, nitrification and DNRA

All treatments were net heterotrophic with a net daily O_2 consumption varying between 21.7 and 37.5 mmol O_2 m^{-2} d^{-1} (Fig. 3). Oxygen fluxes measured in the light and in the dark in control microcosms were not significantly different, and biochar did not produce significant effects on both light and dark O_2 fluxes nor on benthic photosynthesis ($p > 0.1$). Sediments with *V. spiralis* had respiration rates doubling those in unvegetated sediments and rates of gross

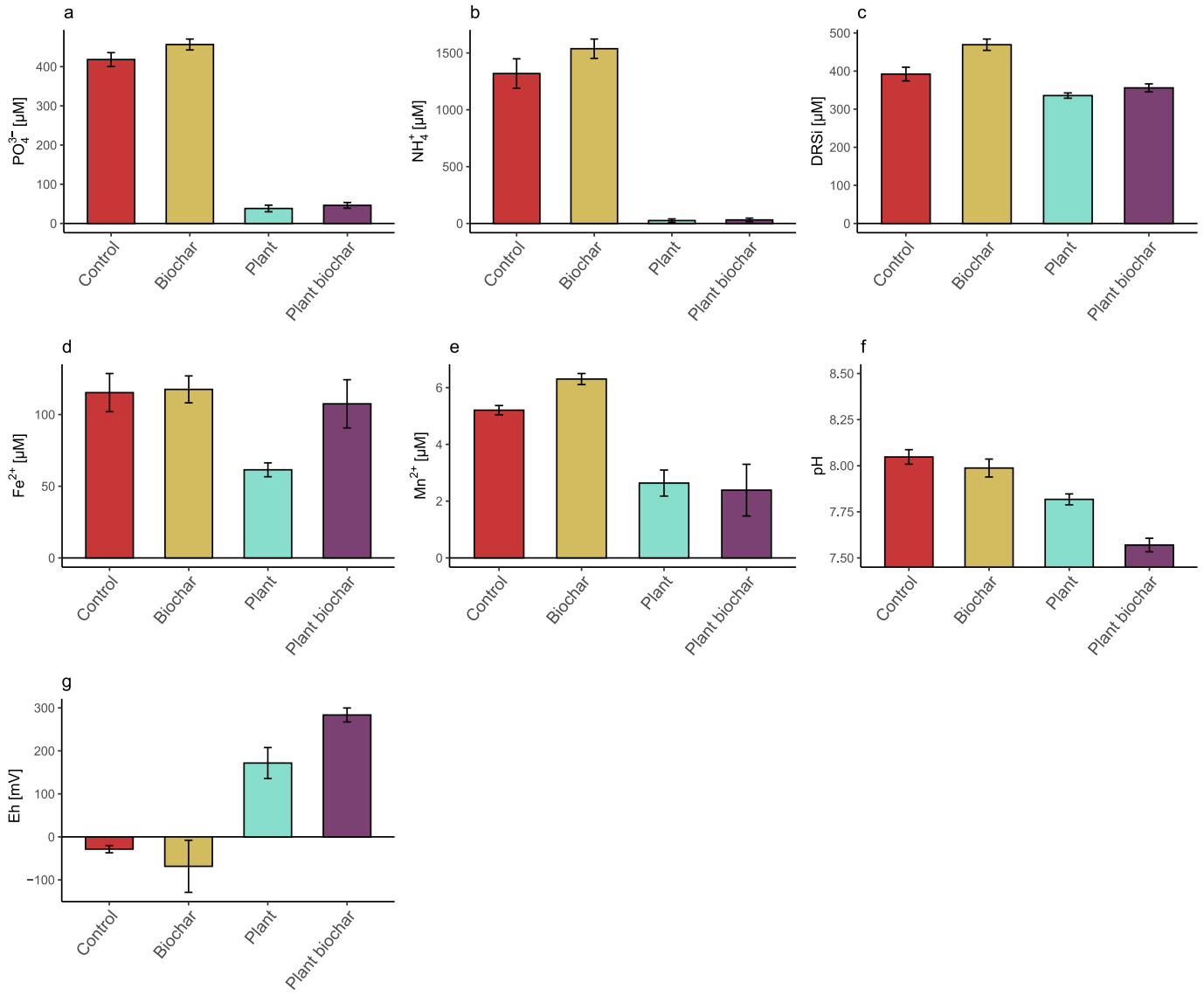

Fig. 2. Pore water chemistry across treatments: a) soluble reactive phosphorus (PO_4^{3-}); b) ammonium (NH_4^+); c) dissolved reactive silica (DRSi); d) dissolved iron (Fe^{2+}); e) dissolved manganese (Mn^{2+}), f) pH and g) Eh.

photosynthesis comparable to benthic respiration rates, resulting in null net primary production ($p < 0.001$; Fig. 3).

The PO_4^{3-} fluxes were characterised by large variability. Anyway, PO_4^{3-} fluxes in the light (-4.9 ± 7.3 µmol m^{-2} h^{-1}) tended to be lower than in the dark (0.5 ± 5.6 µmol m^{-2} h^{-1}; $p < 0.05$). NH_4^+ fluxes were always positive, regardless of the light regime and the presence of biochar or macrophytes and averaged 31.9 ± 20.2 µmol m^{-2} h^{-1}. Vegetated microcosms exhibited higher NH_4^+ release in the dark incubation compared to control sediment, resulting in larger dark ammonium regeneration ($p < 0.05$). Also, DRSi fluxes were characterised by large variability, both in the light (-11.7 ± 75.0 µmol m^{-2} h^{-1}) and in the dark (-1.9 ± 57.0 µmol m^{-2} h^{-1}) and masking regulations by biochar or *V. spiralis*.

The presence of biochar did not affect PD, PN and PDNRA ($p > 0.1$). PD was significantly different between the two layers and in the presence of *V. spiralis* (layer: $p < 0.05$, plant: $p < 0.001$). The highest PD was measured in the 1–5 cm layer of bare sediment microcosms (195.3 ± 36.7 nmol N-N_2 g^{-1} h^{-1}) and the lowest in the vegetated 1–5 cm layer (79.7 ± 49.6 nmol N-N_2 g^{-1} h^{-1}). When both layers of the same treatment were aggregated, bare sediment performed ~4 times higher PD rates compared to vegetated sediments (Fig. 4a). PN had lower rates in the subsurface 1–5 cm layer as compared to the upper sediment layer regardless of the treatment ($p < 0.01$) and the difference between layers was smaller in the presence of *V. spiralis* ($p < 0.05$). The highest PN rate was in the surficial layer of bare sediment (9.5 ± 2.0 nmol N-NO_3^- g^{-1} h^{-1}) and the lowest in the 1–5 cm depth layer of the same treatment (0.4 ± 0.4 nmol N-NO_3^- g^{-1} h^{-1}). Altogether, *V. spiralis* increased PN rates by a factor of ~3, compared to unvegetated microcosms (Fig. 4b). Differently from PN and PD rates, PDNRA was not influenced by *V. spiralis* rhizosphere, but the rates increased significantly along depth ($p < 0.001$; Fig. 4c). Denitrification has the major potential as NO_3^--consuming process in all treatments, with rates higher by at least one order of magnitude than PDNRA (Fig. 4).

3.3. Microbial diversity

All the genetic sequences analysed passed the quality check except for one replicate of superficial vegetated layer not amended with biochar that was discarded.

The 16S rRNA gene amplicon sequencing analysed with DADA2 yielded 21,394 amplicon sequence variants (ASVs) for bacteria and 33,472 for archaea. The Shannon's H alpha diversity was 2.58 ± 0.03 (*n*

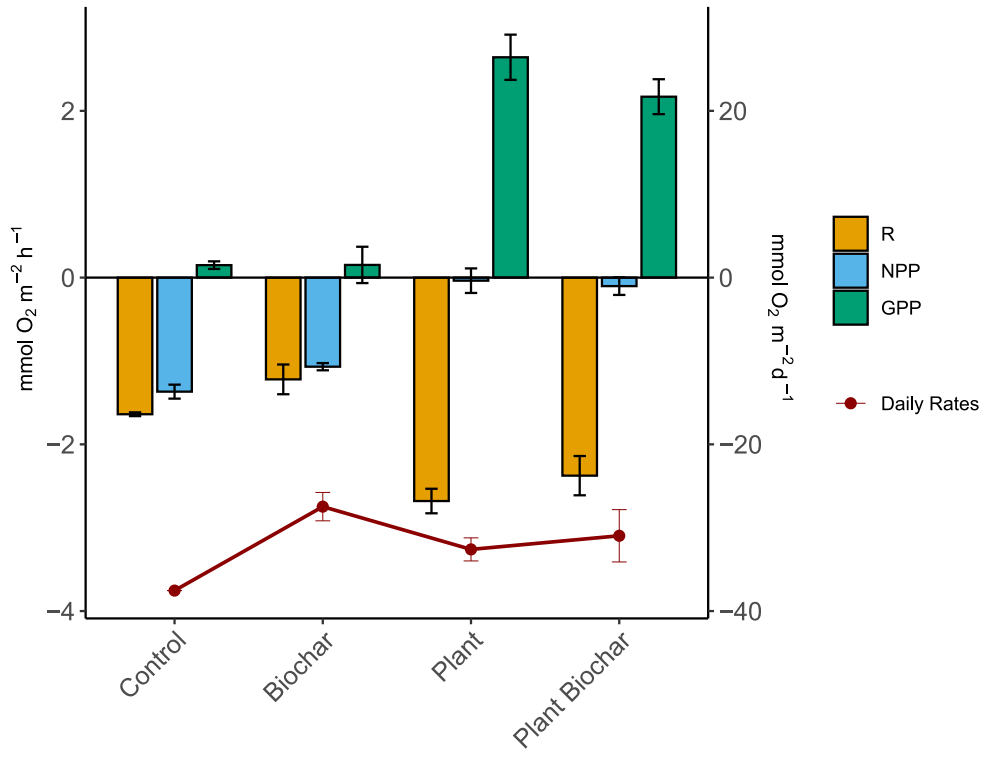

Fig. 3. Hourly net microcosm respiration (R), net primary production (NPP), and gross primary production (GPP) and daily O_2 budget (secondary axis), calculated for a 12 h light and 12 h dark period.

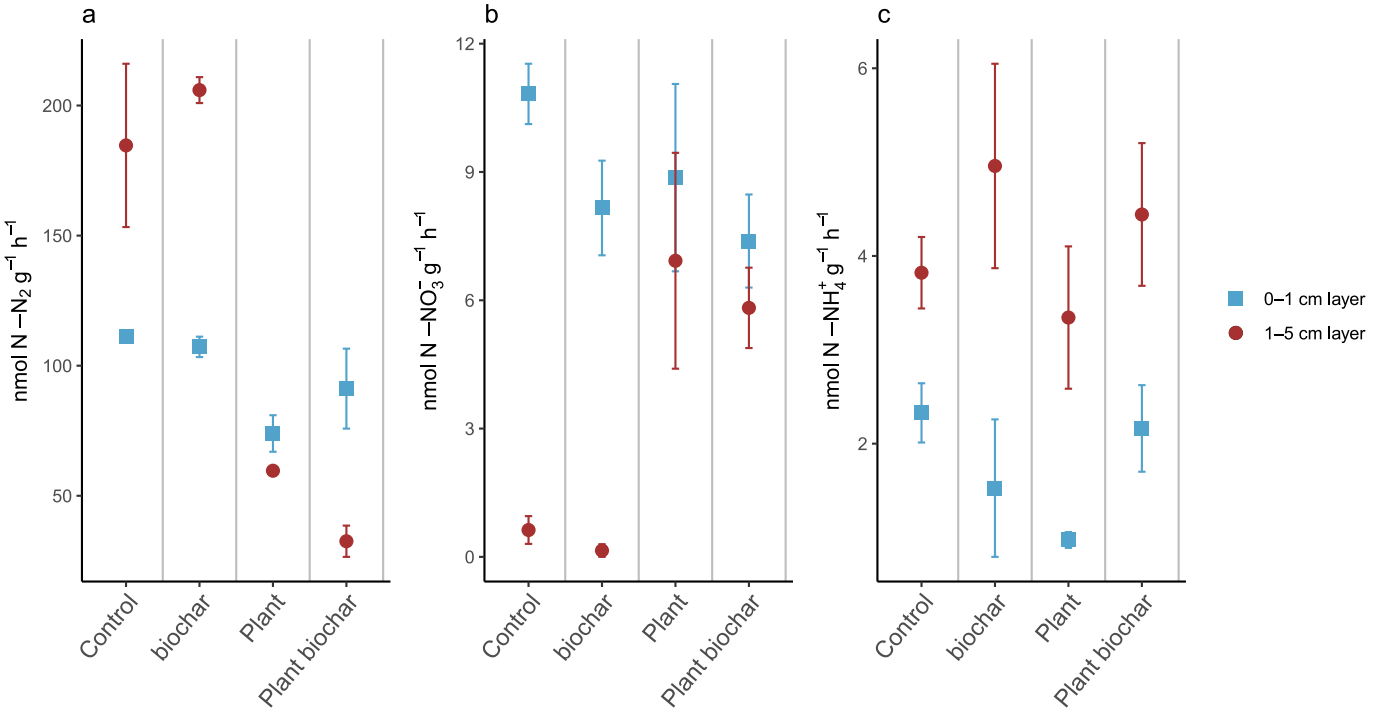

Fig. 4. Potential rates of a) denitrification; b) nitrification and c) DNRA at the two investigated depths. The values are expressed as nmol of N produced per gram of fresh sediment per hour.

= 4) and 0.90 ± 0.01 (n = 4) for bacteria and archaea, respectively. The 16S rRNA gene data Shannon's H alpha diversity (Fig. S3) was significantly lower in the archaea compared to bacteria ($p < 0.0001$). Contrasting the different treatments, archaeal and bacterial Shannon's H diversities were not statistically different.

The relative abundance analysis evidenced that the most abundant Bacteria phyla were Proteobacteria (8.30 ± 42.11 %) and Chloroflexi (2.36 ± 11.98 %), followed by Acidobacteriota (1.50 ± 7.61 %) and Desulfobacteriota (1.46 ± 7.40 %) (Fig. S4). As far as families are concerned, the most dominant families were Competibacteraceae (7.65 ±

33.33 %) and Rhodocyclaceae (1.63 ± 7.07 %).

The amplicon sequencing of Archea showed Crenarchaeota (4.06 ± 39.69 %) as the major phylum, followed by Halobacterota (2.65 ± 25.83 %) and Thermoplasmatota (1.88 ± 18.40 %) (Fig. S4). The most dominant families of Archea were Methanomethyliaceae (1.69 ± 11.59 %), Bathyarchaeia (1.64 ± 11.247 %) and Methanosaetaceae (1.29 ± 8.81 %) (Fig. S4).

As far as the nitrification and denitrification processes are concerned only two bacterial families, Nitrospiraceae and Nitrosomonadaceae, could perform one or more steps of nitrification (ASVs > 0.5 %; Fig. S4; 7). One of the most abundant taxa associated with nitrification was Nitrospira, which can independently carry out both steps of nitrification, converting NH_4^+ to NO_3^-. Additionally, Nitrosomonadaceae oxidizes NH_4^+ to NO_2^-, exhibiting a relative abundance that was positively correlated with PN rates ($p < 0.05$; $r = 0.55$).

The NMDS results of archaea showed no significant distribution patterns. Instead, the NMDS results for bacteria evidenced that the major difference in the overall community composition was driven by sediment depth, while the presence of *V. spiralis* and its roots accounted for a minor role (Fig. 5). Only when single families involved in redox dependent processes that were known to be influenced by ROL were investigated, it was possible to see how the macrophyte presence was a significant factor that shaped the microbial community composition. Nitrosomonadaceae, Nitrospiraceae and Gallionellaceae were always more abundant in the upper sediment layer ($p < 0.001$). In subsurface vegetated sediment their abundance was higher than in bare sediments ($p < 0.05$; Fig. 6a, b, c). Other families were detected exclusively in the presence of *V. spiralis*, suggesting the creation of ecological niches that would not be available without the plant. An example was Beggiatoaceae, comprising sulphate reducing bacteria (Fig. 6d). The microbial community composition was not significantly modified by the biochar addition. Biochar and non-biochar microcosms appear in overlapping clusters in the NMDS graphical representation (Fig. 5).

The relative abundance of the 4 identified putative nitrifying genera was always higher in the superficial layer, where it reached up to 2.3 %. In the subsurface sediment their abundance dropped by a factor of 14 (0.16 ± 0.05 %) in bare microcosms, whereas they decreased much less, by a factor of 3.5, in vegetated sediment (0.64 ± 0.07 %, Fig. 7a). PN rates were positively correlated with the total relative abundance of nitrifying genera ($p < 0.01$, $r = 0.74$; Fig. 7c). In total, 12 genera were detected to be able to perform denitrification. Denitrifiers were always more abundant in the superficial vegetated layer (10.15 ± 0.79 %), ~5 times higher than the nitrifying community (Fig. 7b). PD rates were negatively correlated with the abundance of denitrifying genera ($p < 0.05$, $r = -0.50$; Fig. 7d). The relative abundance of putative iron oxidizing bacteria ($n = 12$ genera) was always higher in the vegetated sediment (6.68 ± 0.93 %) and in the superficial layer (Fig. 8a). The iron oxidizer's relative abundance was positively correlated with the ratio of Fe^{3+} over the total microbially reducible Fe in the sediment ($p < 0.01$, $r = 0.72$; Fig. 8c). The detected bacterial genera involved in iron reduction were always lower than 1.6 % relative abundance. Iron reducing bacteria had higher abundances in the subsurface layer of bare sediments and in the surficial layer of vegetated sediment (Fig. 8b). Five genera were detected that could perform iron reduction suggesting that many of them remained undetected due to the generalized biochemical capacity of microbes to perform this process. The abundance of putative iron reducing bacterial genera was not correlated with the Fe^{3+} percentage over the total Fe pool in the sediment (Fig. 8d).

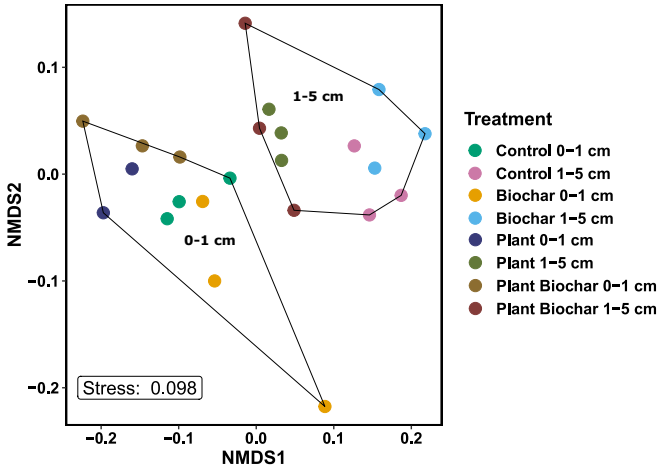

Fig. 5. Beta diversity of the bacterial communities according to a two dimensional non-metric multidimensional scaling (NMDS) on Bray–Curtis dissimilarities. Polygons evidence the clear and not overlapping clustering of the microbial communities in the two investigated depths (0–1 cm, 1–5 cm).

4. Discussion

4.1. Effects of V. spiralis on pore water chemistry

The transplant of *V. spiralis* resulted in a significant reduction of pore water PO_4^{3-}, NH_4^+ and Mn^{2+} as compared to unvegetated microcosms (Fig. 2). This is likely due to active uptake by *V. spiralis* roots, to microbially-mediated or direct oxidation processes, and to precipitation or coprecipitation processes favoured by ROL (Fig. 2) (Brodersen et al., 2018). The reduction of pore water solutes translates into lower concentration gradients with the bottom water and lower diffusive fluxes to the water column, according to Fick's first law of diffusion. For example, sediment-water NH_4^+ fluxes in treatments with *V. spiralis* are expected to be much lower than in non-vegetated sediments, where the absence of roots resulted in 50 times higher pore water NH_4^+ concentration (Fig. 2).

Analogously, the diffusive O_2 uptake is expected to be lower in vegetated microcosms due to higher O_2 concentration in the rhizosphere and to lower concentrations of chemically reduced, O_2 consuming electron donors as Fe^{2+}, sulphides and NH_4^+, affecting redox gradients (Marzocchi et al., 2019; Magri et al., 2023). Marzocchi et al. (2019) quantified ROL by *V. spiralis* in organic sediments via planar oxygen optodes and demonstrated that up to 30 % of the O_2 produced by *V. spiralis* is released from the roots to the sediment. Assuming the same percentage in this experiment, we calculated that nearly 0.37 ± 0.51 mmol m^{-2} h^{-1} of O_2 was released to the rhizosphere via ROL, supporting aerobic microbial respiration, and microbial and/or abiotic oxidation processes. ROL also occurs during the night period, as the plant aerenchyma acts as a conduit for O_2 linking the bottom water with sediments; however, night ROL rates are lower than those measured during light hours (Marzocchi et al., 2019). Significantly higher Eh values in subsurface vegetated than in non-vegetated sediments and lower pore water concentrations of Fe^{2+} and Mn^{2+} support the oxidizing role of *V. spiralis* roots in organic polluted sediments (Fig. 2).

In all microcosms, the measured benthic net fluxes of NH_4^+ and PO_4^{3-} were lower than the calculated diffusive fluxes. This can be explained by the presence of oxic and oxidized sediment layers in the surficial sediment, thicker in vegetated sediment. In such layers NH_4^+ and PO_4^{3-} fluxes can be attenuated by nitrification and coprecipitation with metal oxides, respectively (Soana et al., 2015). Indeed, theoretical diffusive fluxes predict the release of nutrients if biological and abiotic chemical processes are not considered.

Nutrient fluxes in vegetated sediments are affected by factors as uptake and ROL-dependent retention or loss, that tend to reduce regenerative fluxes, and high sediment porosity and ongoing degradation of plant necromass, that can enhance nutrient release (Table 1) (Soana et al., 2015). Additionally, the presence of distinct microbial communities, particularly those growing on roots and leaves as epiphytes, accelerates nutrient cycling through coupled nutrient release and uptake (Brodersen and Kühl, 2022). All these nutrient loops are difficult to quantify and likely explain similar net fluxes in vegetated and

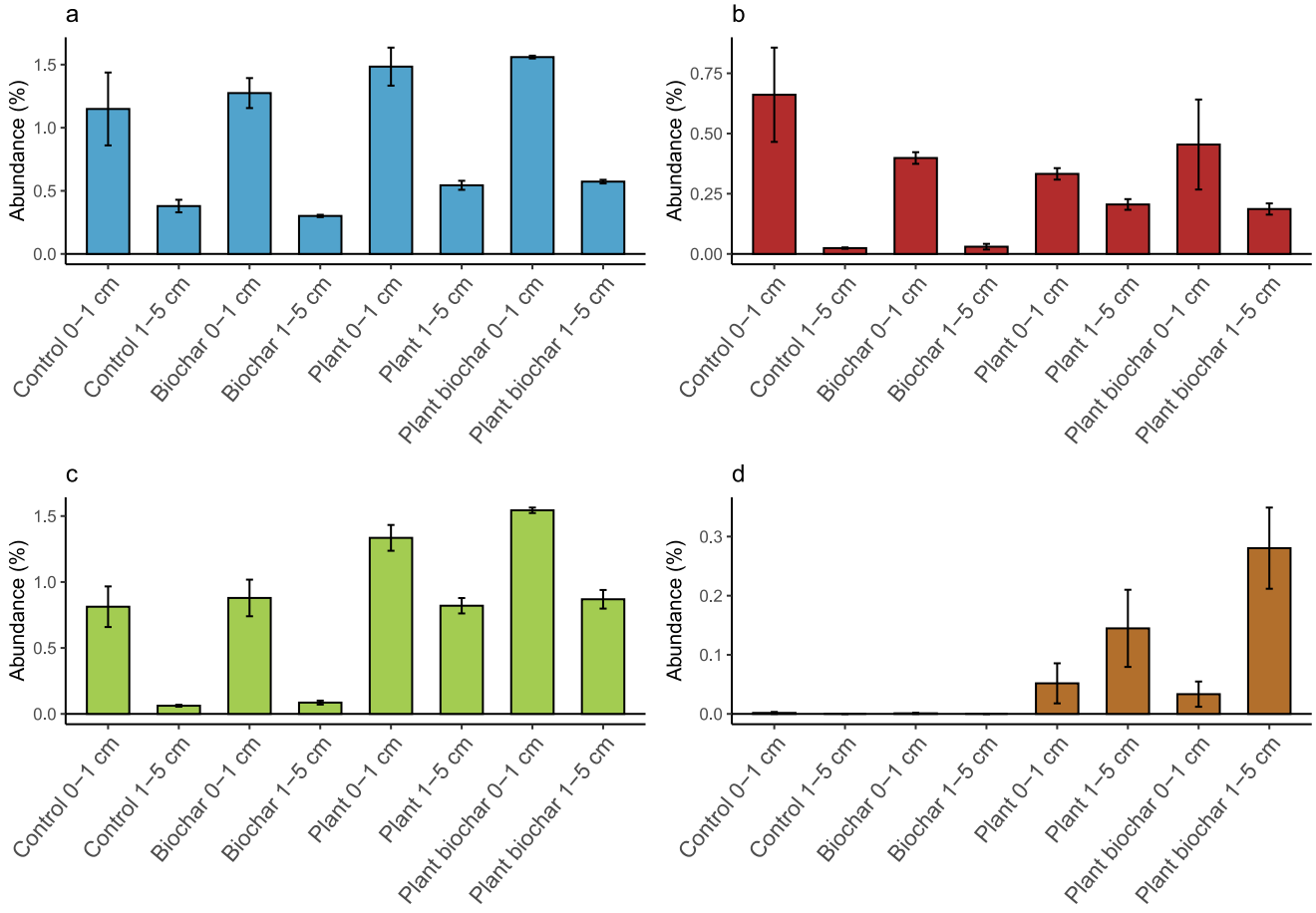

Fig. 6. Relative abundance of the families: a) Nitrosomonadaceae; b) Nitrospiraceae; c) Gallionellaceae; d) Beggiatoaceae. They are expressed as relative abundance over the total bacterial community.

non-vegetated microcosms, hiding much more complex underlying processes in the presence of plants. The measurement of gross nutrient production by *V. spiralis* and sediment and of the assimilation rates of plant roots and leaves via isotopic tracers (Zhang et al., 2010) or planar optodes and gel probes (Scholz et al., 2021) can increase the understanding of nutrient dynamics in vegetated sediments.

4.2. *V. spiralis stimulates the growth of nitrifying bacteria*

Potential nitrification rates in subsurface vegetated sediments were significantly higher than in non-vegetated sediments (Fig. 4). This is due to ROL from macrophyte roots that expands the volume of sediment where nitrifiers can grow below the O_2 penetration depth, which in organic sediments is generally confined to the upper 2–3 mm (Figs. 6, 7) (Risgaard-Petersen and Jensen, 1997; Marzocchi et al., 2019). Similar results are reported for *Vallisneria natans*, which was demonstrated to increase nitrifiers' abundance and nitrification rates in vegetated as compared to unvegetated sediments (Jiang et al., 2024).

The abundance of nitrifiers was positively correlated with the measured potential nitrification rates (Fig. 7a) ($r = 0.73$). Indeed, nitrifiers are a specialized group of slow growing microorganisms, less versatile than other bacteria involved in the nitrogen cycle, as for example denitrifiers (Blackburne et al., 2007). Measurements of potential rates are carried out to quantify the maximum capacity of microorganisms to perform a certain process under non limiting conditions. Measured potential rates are therefore proportional to the number of microbes capable of performing the specific target process. Low rates of potential nitrification in subsurface not vegetated sediments suggest a limited number of nitrifiers, as during measurements sediments are suspended in oxic water with non-limiting concentrations of NH_4^+. Within the microbial community, a few groups can switch their metabolism to nitrification also when the process is thermodynamically favoured (Fig. 4). We are confident that the 16S rDNA analysis detected a major fraction of microorganisms capable of performing nitrification. In fact, if other unaccounted microorganisms were involved in nitrification, the correlation between measured potential rates and microbial abundance would have resulted weaker (Fig. 7a).

Instead, this is likely the explanation for the absence of a significant correlation between potential denitrification and the community of denitrifiers (Fig. 7b). As compared to nitrification genes, denitrification genes are much more widespread among prokaryotes. Many microorganisms inhabiting sediment are versatile, equipped with multiple biochemical pathways and able to switch their heterotrophic metabolism to denitrification in the presence of nitrate (Canfield et al., 2005). In our experiment, the layer with the highest PD was not the layer with the highest relative abundance of denitrifiers, suggesting that some taxa performing denitrification were not detected or described yet, or confirming that genes encoding for denitrification are widespread. Another possible explanation could be the exclusion of *Competibacter* as putative denitrifier; this genus accounts for 20 % of the total bacterial community in the sediment investigated. Some *Competibacter* species, for example *C. denitrificans*, possess denitrification genes, but batch culture experiments confirming this evidence are still lacking (Rubio-Rincón et al., 2017).

The limiting factor for the conversion of NH_4^+ to N_2 through coupled nitrification and denitrification in sediment is the presence of O_2 to support nitrification (Hernández-del Amo et al., 2020). The roots of *V. spiralis* act as a carrier of O_2 that stimulates the growth and the

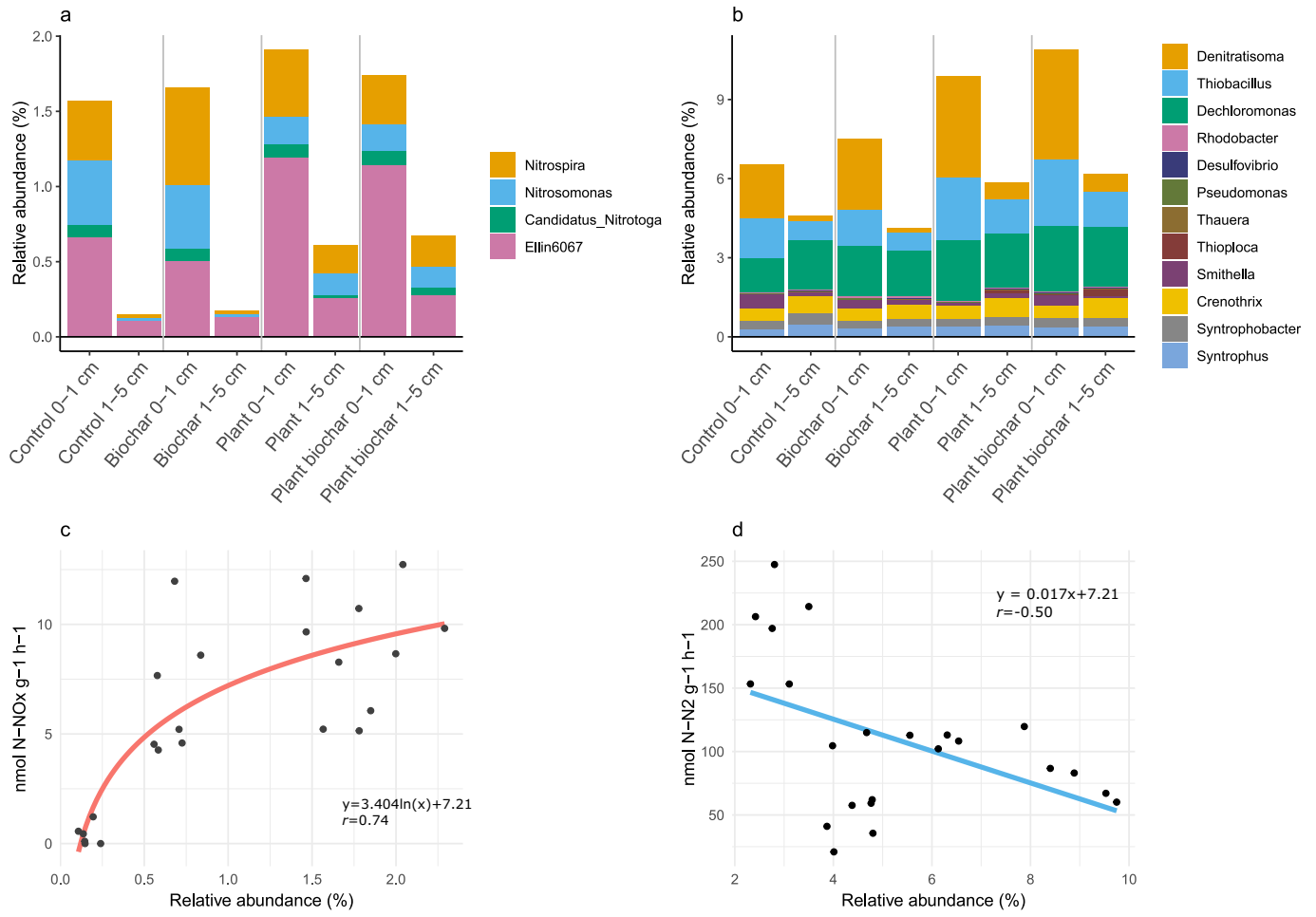

Fig. 7. Relative abundance of the detected bacterial genera that could be involved in a) nitrification and b) denitrification among the total bacterial genera and correlation between measured potential rates of c) nitrification and d) denitrification and the total relative abundance of the bacterial genera involved in the process, respectively.

activity of nitrifiers in subsurface sediments, where this process is generally limited. The produced NO_3^-, diffusing radially to anoxic niches within the rhizosphere, is immediately denitrified due to the widespread denitrification potential of anoxic sediment, even in the absence of NO_3^-. The growth of nitrifiers in the rhizosphere is supported by the different ratio of nitrifiers over denitrifiers in bare (0.04) and vegetated sediments (0.12) (Fig. 7).

Nitrospira was one of the most abundant nitrifiers genera detected in the microcosms. *Nitrospira* can perform the entire process of nitrification converting NH_4^+ to NO_3^- with a process named COMAMMOX (Daims et al., 2015). *Nitrospira*, together with *Nitrosomonas*, that was also detected, are common nitrifiers in the sediments of vegetated wetlands (Pelissari et al., 2018). Another abundant nitrifier is Ellin6067 that can convert NH_4^+ to NO_2^- requiring other bacteria to complete the oxidation to NO_3^- (Sun and Zhu, 2022).

The elevated concentration of sulphides acting as electron donors in organic-rich sediments favours the complete reduction of NO_3^- produced or diffusing a few millimetres below the sediment-water interface (Caffrey et al., 2019). The presence of macrophytes performing ROL favours the growth of nitrifiers at much higher depths, which corresponds to the root penetration depth. In the case of *V. spiralis*, this leads to NO_3^- production in the microcosms down to 5 cm in the sediment. The NO_3^- produced is subsequently reduced by denitrifiers, without NO_3^- accumulation. Vegetated sediments permanently remove for this reason larger amounts of nitrogen than bare sediments (Racchetti et al., 2017). Moreover, *Vallisneria* is also known to frequently host a well-developed epiphytic community able to perform nitrification and denitrification and decrease the NH_4^+ and NO_3^- loads directly in the water column (Jiang et al., 2024).

4.3. *V. spiralis* affects phosphorus availability influencing the iron redox state

The PO_4^{3-} dissolved in pore water is the most reactive and easily available pool of phosphorus in sediments. Simultaneously, PO_4^{3-} in the pore water is orders of magnitude lower than the solid or particulate P pool, making it more susceptible to physical and chemical environmental changes (Hupfer and Lewandowski, 2008). In this experiment, the pore water of the vegetated microcosms was depleted of PO_4^{3-} due to assimilation or coprecipitation in the iron plaques along root surface tissues. ROL generates steep oxic-anoxic gradients determining a cryptic iron cycle where Fe, and P consequently, can be made unavailable (i.e., oxidized and precipitated) or available (i.e., reduced and dissolved) at small spatial and short temporal scales (Li et al., 2024). Such a cryptic cycle net retains Fe, and P within the rhizosphere, preventing their mobilization to the water column.

The total phosphorus pool in the microcosms with *V. spiralis* changed from being partly in soluble form to almost completely as a solid pool concentrated in the rhizosphere where it cannot escape sediments (Magri et al., 2023). This retention mechanism explains why and how rooted macrophytes have the capacity to control phytoplankton growth, which is not only a matter of direct competition but also due to the

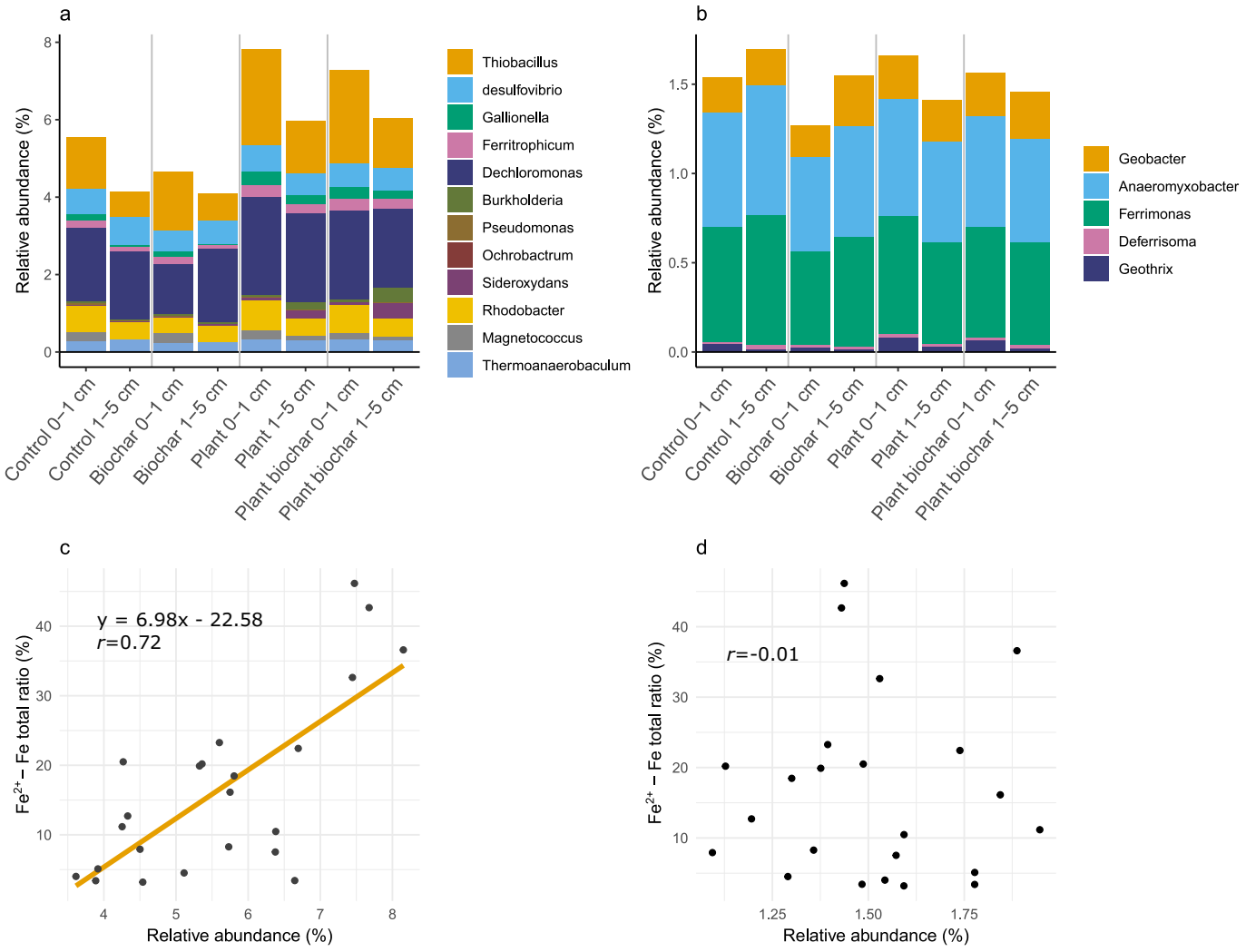

Fig. 8. Relative abundance of the detected bacterial genera that could be involved in a) iron oxidation and b) iron reduction among the total bacterial genera and linear regression of the ratio of microbially reducible Fe^{3+} and the total reactive iron in the sediment and the relative abundance of c) iron oxidizing and d) iron reducing genera respectively.

indirect control of P that is a limiting nutrient (Søndergaard et al., 2017). Moreover, iron plaque deposition and P coprecipitation could represent an adaptive strategy for the plant to survive periods of phosphorus depletion. The iron bound P pool is allocated on the root surface and mechanisms changing local redox conditions or increasing the surface potential of the iron mineral-coated cells allow P mobilization and uptake (Li et al., 2024).

Results from the molecular analyses suggest that in the rhizosphere the microbiologically mediated cycling of iron between reduced and oxidized forms was active. Different microbial groups in the sediment can use Fe^{2+} as an electron donor for chemotrophic metabolism enabling the precipitation of Fe^{3+} minerals, mainly oxyhydroxides, on the root surface. The positive correlation between the ratio of Fe^{3+} over total iron and the relative abundance of putative ferrous iron oxidizing microorganisms support the previous statements (Fig. 8). Among these microorganisms, *Dechloromonas*, *Pseudomonas* and *Thiobacillus* could have genes for denitrification, and they are also able to oxidize iron as an alternative source of energy (Figs. 7, 8) (Hedrich et al., 2011). Other bacteria, for example *Geobacter*, can grow using iron plaques as terminal electron acceptors oxidizing reduced solutes diffusing toward the roots and they should indirectly regulate the provisioning of Fe and P to the roots (Lovley et al., 2011). On the other hand, *Gallionella* was always present and more abundant in surface versus subsurface sediments in the unvegetated sediment, whereas in the presence of *V. spiralis* differences in the abundance of *Gallionalla* between layers were reduced (Fig. 6c). *Gallionella* is known to oxidize iron under neutral pH, precipitating high amounts of iron oxyhydroxide and it is among the bacteria that are able to form iron plaques around roots (Hoover et al., 2023). A similar role is performed by *Syderoxidans* that was also detected in the microcosms.

Besides ensuring P storage and potential availability, the presence of iron plaques on *V. spiralis* and other macrophyte roots may offer additional services. It was recently reported that terrestrial plants favour iron precipitation on the roots as a defensive adaptation against pathogens (Cao et al., 2024). The same can be true for aquatic plants growing in organic sediments. Furthermore, in aquatic plants that must strive in highly reducing sediments, the oxidized iron plaques could act as a barrier to sulphide intrusion in roots. Sulphides react with iron precipitating as FeS or as more stable pyrite in anoxic environments. They can also be oxidized to SO_4^{2-} by the Fe^{3+} that is present in the plaques or by the O_2 provided by roots (Brodersen et al., 2018; Zak et al., 2021). This is confirmed by the decrease of pH due to protons production around roots compared to surrounding sediments. The first reaction could be very important for the survival of the plant when the O_2 provided by roots decreases and it is no longer enough to oxidize the diffusing sulphides. Under these circumstances, the iron plaques represent a reserve of electron acceptors alleviating periods of stress encountered by

macrophytes (Brodersen et al., 2018).

Lower concentrations of total microbially reducible iron and dissolved Fe^{2+} in vegetated as compared to unvegetated microcosms suggest that a significant fraction of the iron pool was converted into iron plaques or oxidized to more stable and less available forms due to processes sustained by ROL (Fig. 1). Furthermore, the increased Fe^{3+} to Fe^{2+} ratio in the superficial vegetated sediments (Fig. 1) suggests higher O_2 penetration depth in sediment with plants compared to bare microcosms, via biogeochemical processes sustained by ROL in subsurface sediments, altering redox gradients (Magri et al., 2023). The same dynamics prevent the diffusion of iron outside the superficial sediment as an explanation of the decreased total iron in vegetated sediments. Loss of Fe^{2+} from the sediment normally happens when the overlying water is depleted of O_2 (Hupfer and Lewandowski, 2008). In this experiment microcosms were always submerged in O_2 saturated and stirred water during preincubation and incubation periods.

4.4. Microbial community composition stresses the importance of sulphur cycle in the rhizosphere

In anoxic sediments of unvegetated microcosms or a few millimetres far from roots, all the inorganic electron acceptors, such as NO_3^-, Mn^{4+}, Fe^{3+} and SO_4^{2-} are expected to be depleted by microbes. Under such circumstances, methanogenesis is the only possible process to gain energy (Borrel et al., 2011). This is confirmed by the high diversity and abundance of methanogens. *Methanosaeta* is the second most abundant genus in all the treatments and *Methanoregula* the fourth most abundant, followed by *Methanolinea*, *Methylotenera* and *Methanobacterium* (Fig. S4). The genetic analyses also revealed that a conspicuous number of procaryotes are in some ways related to the sulphur cycle. Despite any direct measurement of sulphide or sulphate concentrations in the microcosms during the experiment, it is possible to speculate about rhizospheric sulphur cycling and the spatial distribution of the taxa detected from the genetics results.

Beggiatoa includes colourless sulphur bacteria adapted to oxidize sulphides aerobically by living at the interface between oxic and anoxic sediments with sharp redox gradients (Jørgensen and B., 1982). Such gradients are frequently met in cohesive sediments rich in organic matter (Christensen et al., 2000), such as the ones used in this experiment. Interestingly, *Beggiatoa* was detected only in the presence of *V. spiralis* (Fig. 6d), even if all microcosms were preincubated in the same water tank. This suggests a close association between *Beggiatoa* and *V. spiralis* roots, reported also in *Oryza sativa* roots (Pitts et al., 1972). A mutualistic interaction between bacteria and root cells is expected: roots take advantage of the capacity of *Beggiatoa* to oxidize toxic sulphides. In turn, *Beggiatoa* can survive thanks to the O_2 provided by the plant and likely to the labile carbon exudates stimulating sulphate reduction and sulphide production. The presence of a thick surficial sediment layer containing some O_2, NO_3^-, Mn^{4+} and Fe^{3+} may explain the insignificant growth of *Beggiatoa* in the freshwater organic sediment used in the present experiment.

Other bacteria involved in the sulphur cycles are free-living in sediments and not directly associated with *V. spiralis*. For example, members of the family *Desulfosarcinacea* have genes that perform both S reduction and oxidation (Rolando et al., 2024) and they were detected in all the treatments with similar abundance. The other most abundant genera involved in sulphur cycle are *Thiobacillus*, *Sulfurisoma* -a sulphur oxidizer-, and *Sulfuritalea*, that reduce sulphur using NO_3^- as electron acceptor (Fig. S4).

4.5. Biochar exerts a negligible effect on nutrient immobilization

The addition of biochar increased the OM content of the sediment (Table 1); however, such elevated carbon input did not stimulate microbial respiration due to the extremely high C to N ratio and poor nutritional value of the added material (Fig. 3). Biochar is known to increase carbon uptake of submerged plants (Liu et al., 2023). However, TC content of plants was not significantly higher in vegetated microcosms amended with biochar. In the latter, TC of the sediment was lower than in non-vegetated sediments amended with biochar, suggesting that carbon uptake could have happened, but such carbon was consequently respired and not assimilated (Table 1). In soils, biochar increases the TOC and TON content by increasing the water holding capacity of the matrix that favours an increase of microbial biomass (Dong et al., 2016). In the sediment, that is already water saturated, this effect is not expected. Here, the biochar may stimulate the microbial community due to its physical structure favouring biofilm growth.

Experimental evidence points out that biochar addition decreases the total biomass of *Vallisneria* and the mass ratio between roots and leaves (Zheng et al., 2021). This was detected with the addition of biochar exceeding 10 % *v/v*, a value rarely achieved for in-situ amendments due to the high amount of biochar needed to restore ecologically relevant areas. Additions at lower concentrations, but large enough to change physical and chemical properties of the sediment, as in this study (Table 1), are not supposed to affect plant growth rates. Indeed, measured fluxes of O_2 in vegetated sediments with or without biochar addition do not support the hypothesis of higher growth or respiration rates of *V. spiralis* in sediments added with biochar.

Biochar is expected to influence the pH of sediment due to its high alkalinity. The high pH of biochar is explained by the presence of negative functional groups and high carbonate content (Hossain et al., 2020). Interestingly, in this experiment biochar addition significantly decreased the pH of the sediment even if the biochar pH was much higher than the sediment pH (10.0 ± 0.1 versus 8.05 ± 0.04, Fig. 2f). The lowest pH was detected in the sediment with both biochar and *V. spiralis* (7.57 ± 0.04). ROL is known to induce ammonium, iron and sulphide oxidation that are reactions able to release protons. This can explain the decreased pH, but the additive effects given by biochar are still unknown (Brodersen et al., 2018).

Biochar, thanks to its negative surface charge, is considered a more efficient trap for cations and can immobilize on average 20 mg N-NH_4^+ g^{-1} but it produces negligible effects on NO_3^- and it can even favour the release of PO_4^{3-} (Cui et al., 2016). Such effects on nutrients were not detected in this experiment, as evidenced by non-significant differences of NH_4^+ and PO_4^{3-} pore water concentrations in biochar amended and not amended sediments (Fig. 2). It is known that charged organic macromolecules interaction with sorption sites or physical occlusion of biochar pores drastically decrease biochar trapping properties (Feng et al., 2021). The interaction of biochar with the autochthonous elevated content of organic matter in the sediment could have been blocked the active sorption sites of biochar consequently decreasing its nutrient trapping efficiency. The slightly lower total N content in the biochar amended sediments can be explained by the addition of a carbonaceous material with a much lower N content than the surrounding sediment. For this reason, biochar does not act as a source of N for either nitrification or denitrification. The only possible effect of biochar on those processes is due to its physical structure, providing a large colonizable surface for microorganisms (Zhao et al., 2022). However, this is likely to occur only in the proximity of the sediment-water or the sediment-root interfaces, where microorganisms actively performing nitrification and denitrification processes are probably allocated. Here, pronounced O_2 and NO_3^- gradients can sustain quantitatively relevant and coupled redox processes. Biochar is reported to decrease nitrification efficiency in rice paddy soils due to its capacity to immobilize NH_4^+ (Li et al., 2020). In this experiment, biochar had no effect on PN rates. However, more manipulative experiments are needed to confirm these findings, particularly those exploring higher biochar concentrations longer time spans.

Biochar, after its production, can undergo various types of treatments to increase specific characteristics. For example, it can be chemically modified to increase the surface charges and the number of active sorption sites. Some of these treatments consist of physical modification

by microwave action and magnetization to enhance porosity and catalytic activity, or chemical modification by acid or base contact or impregnation in order to enhance ion exchange properties and remove impurities (Amalina et al., 2024). Biochar can be also actively bioengineered inoculating in its matrix specific microorganisms performing processes such as denitrification or nitrification (Zhao et al., 2022). Normally these processes are costly and sometimes they add to biochar chemical substances that in the environment could act as contaminants. For this reason, in the present work it was decided to use unamended biochar without postproduction treatments. This probably impacted on the ability of the carbonaceous material to interact and quantitatively trap ecologically relevant amounts of nutrients from sediments pore water. Non treated biochar with low surface area, porosity and number of active sorption sites should manifest its effects in the benthic environment only after longer times spans compared to the 30 days preincubation performed in the actual experiment (Wei et al., 2024). Alternatively, significant effects can be appreciated if the volumetric amount of biochar added is much higher that the amount used in our experiment (Dong et al., 2016).

Li et al. (2025) report that biochar may act as a terminal electron acceptor in sediments, with a defined maximum capacity to receive electrons from organic matter mineralization processes such as denitrification. Biochar was estimated to be saturated with electrons in only 8 days under optimal conditions for bacterial growth (Li et al., 2025). This means that the biochar employed in the present study may have lost its electron acceptor capacity that needs to be periodically regenerated, and the preincubation time was too long to identify the short-term effect of biochar or respiratory processes as denitrification. The effects of biochar on nutrient concentrations and PN and PD were assessed in this experiment after one month of preincubation when the biochar amendment was supposed to have already lost its positive benefit to the microbial community. Indeed, PN, PD and pore water nutrient concentration were significantly affected by *V. spiralis* and not by biochar (Figs. 2, 4). Therefore, the feasibility of long-term restoration of a eutrophic benthic environment with biochar is expected to be limited in time if not coupled with phytoremediation or other reaeration methods.

The biochar's highest efficiency to trap nutrients was detected in bench scale experiments where sediment cores were capped with a layer mainly composed of biochar (Wei et al., 2023; Zhu et al., 2019). The principle underlying this type of application is different from the one investigated in the actual experiment because it is based on physical nutrient trapping instead of biochemical mineralization. As described in Wei et al. (2023) and Zhu et al. (2019), the lower accumulation of nutrients in the overlying waters of biochar capped cores could be explained by the longest path that dissolved nutrients as NH_4^+ and PO_4^{3-} had to cover before diffusing out of sediment compared to control sediments that had probably only a few mm of O_2 penetration depth and nutrient-rich pore water beneath. Instead, capped cores had presumably an oxic and oxidized biochar layer devoid of dissolved nutrients that smoothed diffusive fluxes from the underlying original sediment. We expected that these positive effects would last only until pore water nutrient concentration in the biochar layer equilibrates with the underlying sediments and the oxidized pool that is able to co-precipitate P is depleted. On the other hand, the planting of *V. spiralis* or other macrophytes that continuously inject O_2 can stimulate the precipitation of metals and P, promote the permanent removal of N and assimilate nutrients trough their roots, acting as a long-term solution compared to biochar capping. Lastly, dry biochar normally has very low density and can float if air bubbles are trapped inside its matrix. The application of biochar over sediment as described in Wei et al. (2023) and Zhu et al. (2019) and not mixed within sediments, seems unpracticable in situ under natural conditions where water currents and wind action are both present, inducing resuspension and mass transport in specific depositional zones. On the other hand, biochar amendment can be faster and easier to carry out as compared to the transplant of macrophytes over large surface areas.

5. Conclusions

Results from this study suggest limited interactions between the relevant biogeochemical ecosystem services provided by *V. spiralis* and biochar in the organic wetland sediment investigated. Biochar addition produced negligible effects on microbial respiration, inorganic nitrogen and phosphorus concentration, and microbial diversity and did not inhibit *V. spiralis* growth and biogeochemical ecosystem services (e.g., its capacity to oxidize sediments via ROL and to selectively stimulate specific oxidative biochemical pathways). Biogeochemical analyses revealed lower concentrations of inorganic nutrients and metals in pore water and different N-related microbial activities in treatments with *V. spiralis*, due to a combination of plant uptake and stimulation of redox processes. Such biogeochemical evidence was supported by genetic analyses, suggesting that plants stimulated microorganisms capable of nitrification, denitrification, iron and sulphur oxidation and reduction. The addition of biochar did not inhibit, nor stimulate in the short term, the services provided by *V. spiralis*, suggesting that the two remediation techniques can be simultaneously applied. As biochar amendments were demonstrated to be effective techniques to contrast heavy metals and hydrocarbon more than nutrient and eutrophication-related contamination, future studies should address whether submerged macrophytes, by adding O_2 and labile exudates to the sediments, inhibit or stimulate the multiple remediation actions and services provided by biochar.

Lastly, the interactions between macrophytes phytoremediation and biochar amendment could be different between plant species and biochar characteristics and along temporal scales, suggesting the need for more in situ and in laboratory experiments.

CRediT authorship contribution statement

Leonardo Morini: Writing – original draft, Methodology, Formal analysis. **Claudio Ferrari:** Writing – original draft, Formal analysis. **Monia Magri:** Writing – review & editing, Formal analysis. **Sara Benelli:** Writing – review & editing, Formal analysis. **Mindaugas Zilius:** Methodology, Formal analysis, Conceptualization. **Giovanna Visioli:** Writing – review & editing, Resources, Funding acquisition. **Marco Bartoli:** Writing – review & editing, Supervision, Resources, Methodology, Funding acquisition, Conceptualization.

Funding sources

This work has benefited from the equipment and framework of the COMP-HUB and COMP-R Initiatives, funded by the 'Departments of Excellence' program of the Italian Ministry for University and Research (MIUR, 2018–2022 and MUR, 2023–2027). This research has financially been supported by the Program "FIL-Quota Incentivante" of the University of Parma and co-sponsored by Fondazione Cariparma.

Declaration of competing interest

The authors have no relevant financial or non-financial interests to disclose.

Appendix A. Supplementary data

Supplementary data to this article can be found online at https://doi.org/10.1016/j.scitotenv.2025.180470.

Data availability

The dataset containing genetic results generated during the current study is available in the NCBI GenBank repository, BioProject PRJNA1107934. The remaining datasets are available from the corresponding author on reasonable request.

References

Amalina, F., Krishnan, S., Zularisam, A.W., Nasrullah, M., 2024. Pristine and modified biochar applications as multifunctional component towards sustainable future: Recent advances and new insights. Sci. Total Environ., 169608 https://doi.org/10.1016/j.scitotenv.2023.169608.

Andrews, S., 2010. FastQC: A Quality Control Tool for High Throughput Sequence Data.

APHA, AWWA, WEF, 2005. Standard Methods for the Examination of Water and Wastewater, 21st ed. American Public Health Association/American Water Works Association/Water Environment Federation. https://doi.org/10.2105/SMWW.2882.089.

Aspila, K.I., Agemian, H., Chau, A.S.Y., 1976. A semi-automated method for the determination of inorganic, organic and total phosphate in sediments. Analyst 101, 187–197. https://doi.org/10.1039/an9760100187.

Blackburne, R., Vadivelu, V.M., Yuan, Z., Keller, J., 2007. Determination of growth rate and yield of nitrifying bacteria by measuring carbon dioxide uptake rate. Water Environ. Res. 79, 2437–2445. https://doi.org/10.2175/106143007x212139.

Borrel, G., Jézéquel, D., Biderre-Petit, C., Morel-Desrosiers, N., Morel, J.P., Peyret, P., Fonty, G., Lehours, A.C., 2011. Production and consumption of methane in freshwater lake ecosystems. Res. Microbiol. 162 (9), 832–847. https://doi.org/10.1016/j.resmic.2011.06.004.

Boucher-Carrier, O., Brisson, J., Abas, K., Duy, S.V., Sauvé, S., Kõiv-Vainik, M., 2022. Effects of macrophyte species and biochar on the performance of treatment wetlands for the removal of glyphosate from agricultural runoff. Sci. Total Environ. 838, 156061. https://doi.org/10.1016/j.scitotenv.2022.156061.

Brodersen, K.E., Kühl, M., 2022. Effects of epiphytes on the seagrass phyllosphere. Front. Mar. Sci. 9, 821614. https://doi.org/10.3389/fmars.2022.821614.

Brodersen, K.E., Kühl, M., Nielsen, D.A., Pedersen, O., Larkum, A.W.D., 2018. Rhizome, root/sediment interactions, aerenchyma and internal pressure changes in seagrasses. In: Larkum, A.W.D., Kendrick, G.A., Ralph, P.J. (Eds.), Seagrasses of Australia: Structure, Ecology and Conservation. Springer, pp. 393–418.

Caffrey, J.M., Bonaglia, S., Conley, D.J., 2019. Short exposure to oxygen and sulfide alter nitrification, denitrification, and DNRA activity in seasonally hypoxic estuarine sediments. FEMS Microbiol. Lett. 366 (1), fny288. https://doi.org/10.1093/femsle/fny288.

Callahan, B.J., McMurdie, P.J., Rosen, M.J., Han, A.W., Johnson, A.J.A., Holmes, S.P., 2016. DADA2: high-resolution sample inference from Illumina amplicon data. Nat. Methods 13, 581–583. https://doi.org/10.1038/nmeth.3869.

Canfield, D.E., Kristensen, E., Thamdrup, B., 2005. The nitrogen cycle. In: Adv. Mar. Biol., 48, pp. 205–267. https://doi.org/10.1016/S0065-2881(05)48007-4.

Cao, M., Platre, M.P., Tsai, H.H., Zhang, L., Nobori, T., Armengot, L., et al., 2024. Spatial IMA1 regulation restricts root iron acquisition on MAMP perception. Nature 625, 750–759. https://doi.org/10.1038/s41586-023-06891-y.

Christensen, P.B., Rysgaard, S., Sloth, N.P., Dalsgaard, T., Schwaerter, S., 2000. Sediment mineralization, nutrient fluxes, denitrification and dissimilatory nitrate reduction to ammonium in an estuarine fjord with sea cage trout farms. Aquat. Microb. Ecol. 21, 73–84. https://doi.org/10.3354/ame021073.

Colmer, T.D., 2003. Long-distance transport of gases in plants: a perspective on internal aeration and radial oxygen loss from roots. Plant Cell Environ. 26, 17–36. https://doi.org/10.1046/j.0016-8025.2002.00846.x.

Cui, X., Hao, H., He, Z., Stoffella, P.J., Yang, X., 2016. Pyrolysis of wetland biomass waste: potential for carbon sequestration and water remediation. J. Environ. Manage. 173, 95–104. https://doi.org/10.1016/j.jenvman.2016.02.049.

Daims, H., Lebedeva, E.V., Pjevac, P., et al., 2015. Complete nitrification by Nitrospira bacteria. Nature 528, 504–509. https://doi.org/10.1038/nature16461.

Deng, S., Chen, J., Chang, J., 2021. Application of biochar as an innovative substrate in constructed wetlands/biofilters for wastewater treatment: performance and ecological benefits. J. Clean. Prod. 293, 126156. https://doi.org/10.1016/j.jclepro.2021.126156.

Dong, X., Guan, T., Li, G., Lin, Q., Zhao, X., 2016. Long-term effects of biochar amount on the content and composition of organic matter in soil aggregates under field conditions. J. Soil. Sediment. 16 (5), 1481–1497. https://doi.org/10.1007/s11368-015-1338-5.

Ewels, P., Magnusson, M., Lundin, S., Käller, M., 2016. MultiQC: summarize analysis results for multiple tools and samples in a single report. Bioinformatics 32, 3047–3048. https://doi.org/10.1093/bioinformatics/btw354.

Feng, Z., Fan, Z., Song, H., Li, K., Lu, H., Liu, Y., Cheng, F., 2021. Biochar induced changes of soil dissolved organic matter: the release and adsorption of dissolved organic matter by biochar and soil. Sci. Tot. Environ. 783. https://doi.org/10.1016/j.scitotenv.2021.147091.

Galitskaya, P., Akhmetzyanova, L., Selivanovskaya, S., 2016. Biochar-carrying hydrocarbon decomposers promote degradation during the early stage of bioremediation. Biogeosciences 13, 5739–5752. https://doi.org/10.5194/bg-13-5739-2016.

Hedrich, S., Schlömann, M., Barrie Johnson, D., 2011. The iron-oxidizing proteobacteria. Microbiology 157, 1551–1564. https://doi.org/10.1099/mic.0.045344-0.

Hernández-del Amo, E., Dolinová, I., la Ramis-Jorba, G., Gich, F., Bañeras, L., 2020. Limited effect of radial oxygen loss on ammonia oxidizers in *Typha angustifolia* root hairs. Sci. Rep. 10. https://doi.org/10.1038/s41598-020-72653-9.

Hoover, R.L., Keffer, J.L., Polson, S.W., Chan, C.S., 2023. Gallionellaceae pangenomic analysis reveals insight into phylogeny, metabolic flexibility, and iron oxidation mechanisms. mSystems 8. https://doi.org/10.1128/msystems.00038-23.

Hossain, M.Z., Bahar, M.M., Sarkar, B., Donne, S.W., Ok, Y.S., Palansooriya, K.N., Kirkham, M.B., Chowdhury, S., Bolan, N., 2020. Biochar and its importance on nutrient dynamics in soil and plant. Biochar 2, 379–420. https://doi.org/10.1007/s42773-020-00065-z.

Hupfer, M., Lewandowski, J., 2008. Oxygen controls the phosphorus release from lake sediments - a long-lasting paradigm in limnology. Int. Rev. Hydrobiol. 93, 415–432. https://doi.org/10.1002/iroh.200711054.

Jiang, X., Wang, M., He, D., Zhu, J., Yang, S., Fang, F., Yang, L., 2024. Submerged macrophyte promoted nitrogen removal function of biofilms in constructed wetland. Sci. Total Environ. 914, 169666. https://doi.org/10.1016/j.scitotenv.2023.169666.

Jørgensen, B., B., J., 1982. Ecology of the bacteria of the sulphur cycle with special reference to anoxic-oxic interface environments. Trans. R. Soc. Lond. B. 298, 543–561. https://www.jstor.org/stable/2395814.

Li, F., Liang, X., He, S., Li, M., Cao, Y., Zhang, J., Tian, G., 2020. Biochar slows gross nitrification and gasses N emission via lower autotrophic nitrification in paddy soils. J. Soils & Sediments 20, 629–640. https://doi.org/10.1007/s11368-019-02445-w.

Li, J., Zhang, Y., Zhang, W., 2024. Biochemical mechanisms underlying iron plaque-mediated phosphorus accumulation and uptake in rice roots. Sci. Total Environ. 929, 172331. https://doi.org/10.1016/j.scitotenv.2024.172331.

Li, W., Keffer, J.L., Singh, A., Chan, C.S., Chiu, P.C., 2025. Mechanism and capacity of black carbon (biochar) to support microbial growth. Biogeochemistry 168 (2). https://doi.org/10.1007/s10533-025-01221-y.

Liu, Z., Zhang, W., Ma, R., Li, S., Song, K., Zheng, J., Wang, Y., Bian, R., Zhang, X., Pan, G., 2023. Biochar-plant interactions enhance nonbiochar carbon sequestration in a rice paddy soil. Commun. Earth Environ. 4, 494. https://doi.org/10.1038/s43247-023-01155-z.

Lorenzen, C.J., 1967. Determination of chlorophyll and pheo pigments: spectrophotometric equations. Limnol. Oceanogr. 12 (2), 343–346. https://doi.org/10.4319/lo.1967.12.2.0343.

Lovley, D.R., Phillips, E.J.P., 1987. Rapid assay for microbially reducible ferric iron in aquatic sediments. Appl. Environ. Microbiol. 53 (7). https://doi.org/10.1128/aem.53.7.1536-1540.1987.

Lovley, D.R., Ueki, T., Zhang, T., Malvankar, N.S., Shrestha, P.M., Flanagan, K.A., Aklujkar, M., Butler, J.E., Giloteaux, L., Rotaru, A.E., Holmes, D.E., Franks, A.E., Orellana, R., Risso, C., Nevin, K.P., 2011. Geobacter. The Microbe Electric's Physiology, Ecology, and Practical Applications. In: Advances in Microbial Physiology. Academic Press, pp. 1–100. https://doi.org/10.1016/B978-0-12-387661-4.00004-5.

Magri, M., Benelli, S., Bartoli, M., 2023. *Vallisneria spiralis* promotes P and Fe retention via radial oxygen loss in contaminated sediments. Water (Basel) 15 (4222). https://doi.org/10.3390/w15244222.

Marzocchi, U., Benelli, S., Larsen, M., Bartoli, M., Glud, R.N., 2019. Spatial heterogeneity and short-term oxygen dynamics in the rhizosphere of *Vallisneria spiralis*: implications for nutrient cycling. Freshw. Biol. 64, 532–543. https://doi.org/10.1111/fwb.13240.

Morini, L., Ferrari, C., Bartoli, M., Zilius, M., Broman, E., Visioli, G., 2024. *Vallisneria spiralis* L. adaptive capacity improves pore water chemistry and increases potential nitrification in organic polluted sediments. Ecol. Process. 13. https://doi.org/10.1186/s13717-024-00506-8.

Pelissari, C., Guivernau, M., Viñas, M., García, J., Velasco-Galilea, M., Souza, S.S., Sezerino, P.H., Ávila, C., 2018. Effects of partially saturated conditions on the metabolically active microbiome and on nitrogen removal in vertical subsurface flow constructed wetlands. Water Res. 141, 185–195. https://doi.org/10.1016/j.watres.2018.05.002.

Pitts, G., Allam, A.I., Hollis, J.P., 1972. *Beggiatoa*: occurrence in the rice rhizosphere. Science 178, 990–992. https://doi.org/10.1126/science.178.4064.990.

Quast, C., Pruesse, E., Yilmaz, P., Gerken, J., Schweer, T., Yarza, P., Peplies, J., Glöckner, F.O., 2012. The SILVA ribosomal RNA gene database project: improved data processing and web-based tools. Nucl. Acids Res. 41, D590–D596. https://doi.org/10.1093/nar/gks1219.

Racchetti, E., Longhi, D., Ribaudo, C., Soana, E., Bartoli, M., 2017. Nitrogen uptake and coupled nitrification–denitrification in riverine sediments with benthic microalgae and rooted macrophytes. Aquat. Sci. 79, 487–505. https://doi.org/10.1007/s00027-016-0512-1.

Risgaard-Petersen, N., Jensen, K., 1997. Nitrification and denitrification in the rhizosphere of the aquatic macrophyte *Lobelia dortmanna* L. Limnol. Oceanogr. 42, 529–537. https://doi.org/10.4319/lo.1997.42.3.0529.

Robertson, C.E., Harris, J.K., Wagner, B.D., Granger, D., Browne, K., Tatem, B., Feazel, L. M., Park, K., Pace, N.R., Frank, D.N., 2013. Explicet: graphical user interface software for metadata-driven management, analysis and visualization of microbiome data. Bioinformatics 29, 3100–3101. https://doi.org/10.1093/bioinformatics/btt526.

Rolando, J.L., Kolton, M., Song, T., Liu, Y., Pinamang, P., Conrad, R., Morris, J.T., Konstantinidis, K.T., Kostka, J.E., 2024. Sulfur oxidation and reduction are coupled to nitrogen fixation in the roots of the salt marsh foundation plant Spartina alterniflora. Nat. Commun. 15 (1). https://doi.org/10.1038/s41467-024-47646-1.

RStudio Team, 2023. RStudio: Integrated Development for R. RStudio. http://www.rstudio.com/.

Rubio-Rincón, F.J., Lopez-Vazquez, C.M., Welles, L., van Loosdrecht, M.C.M., Brdjanovic, D., 2017. Cooperation between *Candidatus Competibacter* and *Candidatus Accumulibacter* clade I, in denitrification and phosphate removal processes. Water Res. 120, 156–164. https://doi.org/10.1016/j.watres.2017.05.001.

Sand-Jensen, K., Prahl, C., Stokholm, H., 1982. Oxygen release from roots of submerged aquatic macrophytes. Oikos 38, 349–354. https://doi.org/10.2307/3544675.

Soana, E., Naldi, M., Bonaglia, S., Racchetti, E., Castaldelli, G., Brüchert, V., Viaroli, P., Bartoli, M., 2015. Benthic nitrogen metabolism in a macrophyte meadow (*Vallisneria spiralis* L.) under increasing sedimentary organic matter loads. Biogeochemistry 124, 387–404. https://doi.org/10.1007/s10533-015-0104-5.

Søndergaard, M., Lauridsen, T.L., Johansson, L.S., Jeppesen, E., 2017. Nitrogen or phosphorus limitation in lakes and its impact on phytoplankton biomass and

submerged macrophyte cover. Hydrobiologia 795, 35–48. https://doi.org/10.1007/s10750-017-3110-x.
Stocum, E.T., Plante, C.J., 2006. The effect of artificial defaunation on bacterial assemblages of intertidal sediments. J. Exp. Mar. Biol. Ecol. *337* (2), 147–158. https://doi.org/10.1016/j.jembe.2006.06.012.
Sun, Q., Zhu, G., 2022. Deciphering the effects of antibiotics on nitrogen removal and bacterial communities of autotrophic denitrification systems in a three-dimensional biofilm electrode reactor. Environ. Pollut. 315, 120476. https://doi.org/10.1016/J.ENVPOL.2022.120476.
Thomaz, S.M., 2023. Ecosystem services provided by freshwater macrophytes. Hydrobiologia 850, 2757–2777. https://doi.org/10.1007/s10750-021-04739-y.
Scholz, V.v., Brodersen, K.E., Kühl, M., Koren, K., 2021. Resolving chemical gradients around seagrass roots—a review of available methods. Front. Mar. Sci. 8, 771382. https://doi.org/10.3389/fmars.2021.771382.
Valderrama, J.C., 1981. The simultaneous analysis of total nitrogen and total phosphorus in natural waters. Mar. Chem. 10. https://doi.org/10.1016/0304-4203(81)90027-X.
Vila-Costa, M., Pulido, C., Chappuis, E., Calviño, A., Casamayor, E.O., Gacia, E., 2016. Macrophyte landscape modulates lake ecosystem-level nitrogen losses through tightly coupled plant-microbe interactions. Limnol. Oceanogr. 61, 78–88. https://doi.org/10.1002/lno.10209.
Vörösmarty, C.J., McIntyre, P.B., Gessner, M.O., Dudgeon, D., Prusevich, A., Green, P., Glidden, S., Bunn, S.E., Sullivan, C.A., Liermann, C.R., Davies, P.M., 2010. Global threats to human water security and river biodiversity. Nature 467, 555–561. https://doi.org/10.1038/nature09440.
Warembourg, F.R., 1993. Nitrogen fixation in soil and plant systems. Nitrogen Isotope Techniques. Academic Press, pp. 127–156.
Wei, L., Zhang, Y., Han, Y., Zheng, J., Xu, X., Zhu, L., 2023. Effective abatement of ammonium and nitrate release from sediments by biochar coverage. Sci. Total Environ. 899, 165710. https://doi.org/10.1016/j.scitotenv.2023.165710.
Wei, J., Qin, G., Zeng, Q., Luo, Q., Ji, J., Yan, X., Wu, J., Wei, Z., 2024. Biochar effects on soil aggregation, phosphorus distribution, and colloidal phosphorus content in paddy soils: a comparative study. J. Soil. Sediment. 24, 2237–2247. https://doi.org/10.1007/s11368-024-03821-x.
Zak, D., Hupfer, M., Cabezas, A., Jurasinski, G., Audet, J., Kleeberg, A., McInnes, R., Kristiansen, S.M., Petersen, R.J., Liu, H., Goldhammer, T., 2021. Sulphate in freshwater ecosystems: a review of sources, biogeochemical cycles, ecotoxicological effects and bioremediation. Earth Sci. Rev. 212. https://doi.org/10.1016/j.earscirev.2020.103446.
Zamparas, M., Zacharias, I., 2014. Restoration of eutrophic freshwater by managing internal nutrient loads. A review. Sci. Total Environ. 496, 551–562. https://doi.org/10.1016/j.scitotenv.2014.07.076.
Zhang, L., Li, K., Liu, Z., Middelburg, J.J., 2010. Sedimented cyanobacterial detritus as a source of nutrient for submerged macrophytes (*Vallisneria spiralis* and *Elodea nuttallii*): an isotope labeling experiment using ^{15}N. Limnol. Oceanogr. *55* (5), 1912–1917. https://doi.org/10.4319/lo.2010.55.5.1912.
Zhao, L., Fu, G., Pang, W., Tang, J., Guo, Z., Hu, Z., 2022. Biochar immobilized bacteria enhances nitrogen removal capability of tidal flow constructed wetlands. Sci. Total Environ. 836, 155728. https://doi.org/10.1016/j.scitotenv.2022.155728.
Zheng, C., Zhang, X., Gan, L., He, Z., Zhu, J., Zhang, W., Gao, Y., Yang, L., 2021. Effects of biochar on the growth of *Vallisneria natans* in surface flow constructed wetland. Environ. Sci. Pollut. Res. 28, 66158–66170. https://doi.org/10.1007/s11356-021-15399-9.
Zhu, Y., Tang, W., Jin, X., Shan, B., 2019. Using biochar capping to reduce nitrogen release from sediments in eutrophic lakes. Sci. Total Environ. 646, 93–104. https://doi.org/10.1016/j.scitotenv.2018.07.277.